

Article

# Influence of the Support on Propene Oxidation over Gold Catalysts

Ewoud J. J. de Boed, Bryan J. Folmer, Min Tang, Baira Donoeva and Petra E. de Jongh \*

Materials Chemistry and Catalysis, Debye Institute for Nanomaterials Science, Utrecht University, Universiteitsweg 99, 3584 CG Utrecht, The Netherlands; e.j.j.deboed@uu.nl (E.J.J.d.B.); b.j.folmer@uu.nl (B.J.F.); m.tang@uu.nl (M.T.); baira.donoeva@gmail.com (B.D.)

\* Correspondence: p.e.dejongh@uu.nl

**Abstract:** The epoxidation of propene without forming a substantial amount of byproducts is one of the holy grails of catalysis. Supported Cu, Ag and Au catalysts are studied for this reaction and the activity of the supported metals is generally well understood. On the contrary, limited information is available on the influence of the support on the epoxide selectivity. The reaction of propene with equal amounts of hydrogen and oxygen was tested over gold nanoparticles deposited onto CeO<sub>2</sub>, TiO<sub>2</sub>, WO<sub>3</sub>,  $\gamma$ -Al<sub>2</sub>O<sub>3</sub>, SiO<sub>2</sub>, TiO<sub>2</sub>-SiO<sub>2</sub> and titanosilicate-1. Several metal oxide supports caused further conversion of the synthesized propene oxide. Strongly acidic supports, such as WO<sub>3</sub> and titanosilicate-1, catalyzed the isomerization of propene oxide towards propanal and acetone. Key factors for achieving high PO selectivity are having inert or neutralized surface sites, a low specific surface and/or a low density of surface -OH groups. This work provides insights and practical guidelines to which metal oxide support properties lead to which products in the reaction of propene in the presence of oxygen and hydrogen over supported gold catalysts.

**Keywords:** epoxidation; propene oxide; gold nanoparticles; support effects



**Citation:** de Boed, E.J.J.; Folmer, B.J.; Tang, M.; Donoeva, B.; de Jongh, P.E. Influence of the Support on Propene Oxidation over Gold Catalysts. *Catalysts* **2022**, *12*, 327. <https://doi.org/10.3390/catal12030327>

Academic Editors: Vincenzo Russo, Pasi Tolvanen and Sébastien Leveneur

Received: 8 February 2022

Accepted: 9 March 2022

Published: 11 March 2022

**Publisher's Note:** MDPI stays neutral with regard to jurisdictional claims in published maps and institutional affiliations.

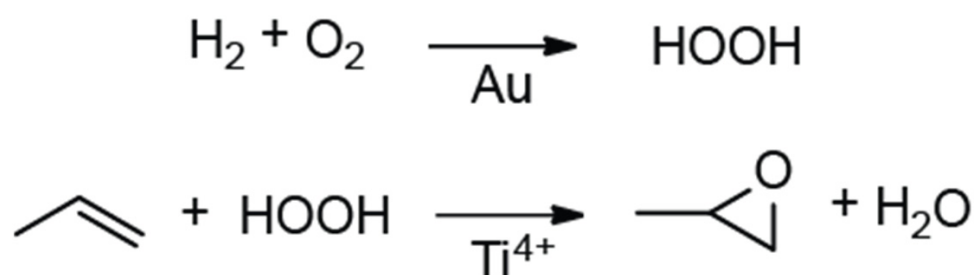


**Copyright:** © 2022 by the authors. Licensee MDPI, Basel, Switzerland. This article is an open access article distributed under the terms and conditions of the Creative Commons Attribution (CC BY) license (<https://creativecommons.org/licenses/by/4.0/>).

## 1. Introduction

Propene oxide (PO) is a chemical intermediate that is widely used in the production of a variety of derivatives, including polyether polyols and propene glycol [1,2]. Currently, PO is produced via two industrial processes: the chlorohydrin process and the hydroperoxide process. The chlorohydrin route suffers from the production of chlorinated byproducts that pose environmental issues, while the hydroperoxide route suffers from the mismatch in the market demand of co-products such as styrene monomer and methyl-*tert*-butylether [1]. Hence the direct epoxidation of propene with O<sub>2</sub> (and H<sub>2</sub>) to offer PO without byproducts would be a very attractive option and has received much attention in academia and industry.

In their initial study, Haruta and co-workers reported that Au/TiO<sub>2</sub> and Au/TiO<sub>2</sub>-SiO<sub>2</sub> were active and selective catalysts for propene epoxidation with O<sub>2</sub> in the presence of H<sub>2</sub>. From the supported metals studied, gold was the only metal active and selective for PO formation [3]. Since then, the Au catalyzed propene epoxidation with H<sub>2</sub> and O<sub>2</sub> has been studied in more detail. Scheme 1 shows the generally accepted mechanism. Au activates H<sub>2</sub> and O<sub>2</sub> to form a peroxide, this is considered the rate determining step [4]. The peroxide is spilt over to a Ti<sup>4+</sup>-OH site at the interface between the Au nanoparticle and TiO<sub>2</sub> support. Electrophilic oxygen transfer can occur from the Ti<sup>4+</sup>-OOH to the C=C bond to yield PO and Ti<sup>4+</sup>-OH and form a stoichiometric amount of H<sub>2</sub>O as the only by-product [5–8]. Au is thus essential for the activation of H<sub>2</sub> and O<sub>2</sub>, while PO is formed at the interface between Au and the surface of the support.



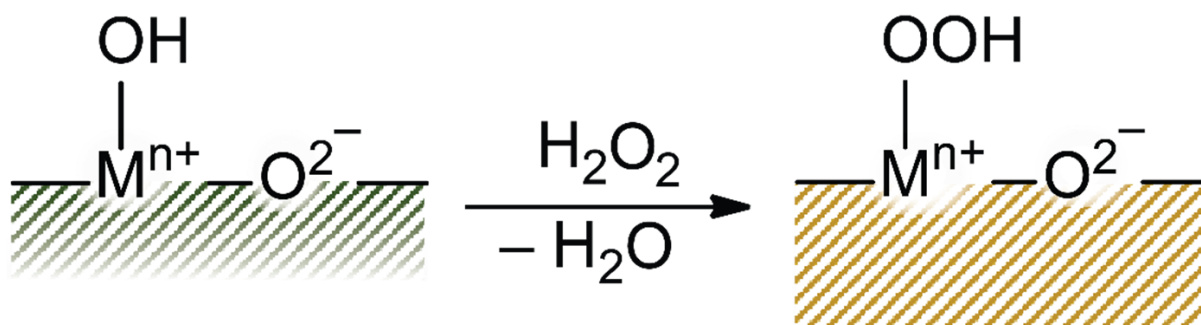
**Scheme 1.** Reaction mechanism of Au-Ti catalyzed propene epoxidation.

Au-Ti<sup>4+</sup> catalyzed propene epoxidation is structure sensitive: only gold particles smaller than 5 nm are active and selective for propene epoxidation [9]. The PO turnover frequency (TOF) of titanosilicate-1 (TS-1) supported gold catalysts with varying gold particle size depends as  $d^{-2.7}$  on the average Au diameter  $d$ , being related to the corner sites of the Au particle. The larger particles of 5.1 nm in the study by Yuan and co-workers show a TOF of ca. 0.02 mole PO produced per mole Au surface-atoms per second ( $\text{s}^{-1}$ ) at 200 °C. The smaller gold particles of 2.6 nm show a TOF of ca.  $0.14 \text{ s}^{-1}$  at the same temperature, which clearly indicates the size dependency [9,10]. In addition, Oyama et al. showed that only neutral gold particles catalyze the propene epoxidation while cationic gold(III) oxide particles of 3 nm catalyze propene hydrogenation under the same reaction conditions [11]. Next to gold particle size and charge, also the surface properties of the Ti<sup>4+</sup>-based supports such as reducibility and acidity/basicity are important. The effect of metal oxide supports on Au-catalyzed propene epoxidation is not yet well understood.

Metal oxide supports show a wide range of physicochemical properties including different morphology (pore structure and accessibility of active sites), reducibility of the metal cations in the oxide and acid/base properties. Firstly, transition metal oxides are often redox active, which is essential for catalysis of oxidation reactions that follow a Mars-van-Krevelen-mechanism [12,13]. The redox-activities of transition metal oxides enhance the availability of active O-species of the support and explain the high activity of Au/CeO<sub>2</sub> catalysts in CO and volatile organic chemical oxidations [14–16]. Besides CeO<sub>2</sub>, other examples of reducible supports include many transition metal oxides, including CrO<sub>3</sub>, V<sub>2</sub>O<sub>5</sub>, WO<sub>3</sub>, MnO<sub>2</sub> and Fe<sub>3</sub>O<sub>4</sub> [12,17,18]. Conversely,  $\alpha$ -Al<sub>2</sub>O<sub>3</sub>,  $\gamma$ -Al<sub>2</sub>O<sub>3</sub> and SiO<sub>2</sub> are typical examples of inert and non-reducible oxides [12,17].

Secondly, the acid/base properties of metal oxide supports can be divided by their nature, e.g., protonic/non-protonic, their strength and density. Due to the high electron deficiency of the metal cations that are present in metal oxides, oxides of transition metals are well known to accept electrons and to have non-protonic/Lewis acids sites on the surface, such as is the case on for instance TiO<sub>2</sub>, MoO<sub>3</sub> or  $\gamma$ -Al<sub>2</sub>O<sub>3</sub> [19–22]. On the contrary, surface hydroxyl groups tend to act as protonic/Brønsted acids. Adsorption of pyridine or ammonia on Brønsted acid metal oxides, such as Nb<sub>2</sub>O<sub>5</sub> or WO<sub>3</sub>, results in the formation of pyridinium and ammonium ions, respectively [23–25]. The strength of both types of acid sites depends on structural parameters, composition and contamination of the metal oxide and oxidation state and electronegativity of the elements that compose the metal oxide. Adsorption with probe molecules can be used for the determination of the acid strength and is in addition one of the tools to determine the density of acidic sites on the surface of metal oxides [26]. Another viable parameter that describes the acidity is the point-of-zero-charge (PZC). The PZC indicates that a metal oxide is overall acidic with a PZC  $\ll$  pH 7 or basic with a PZC  $\gg$  pH 7 or amphoteric with a PZC  $\pm$  pH 7. An amphoteric metal oxide contains both acidic and basic sites [27].

Most studies on Au catalyzed propene epoxidation are based on the use of  $\text{Ti}^{4+}$  containing supports, such as  $\text{TiO}_2$ ,  $\text{TiO}_2\text{-SiO}_2$  and titanosilicate-1 (TS-1). The formation of  $\text{Ti}^{4+}\text{-OOH}$  species is crucial for the propene epoxidation reaction as depicted in Scheme 2.  $\text{Ti}^{4+}\text{-OOH}$  species are both observed in the gold catalyzed propene epoxidation in the gas phase [7,28] and in the liquid phase epoxidation of propene with aqueous  $\text{H}_2\text{O}_2$  [29,30]. Next to  $\text{TiO}_2$ , other metal oxides with Lewis acid sites are also reported to activate  $\text{H}_2\text{O}_2$  in a similar fashion, but are typically studied in liquid phase reactions. Examples of such metal oxides include  $\text{WO}_3$  and soluble  $\text{W}^{6+}$  compounds [25,31]. Solid  $\text{WO}_3$  has been studied as a support for Ag catalyzed epoxidations, but not for the gold catalyzed propene epoxidation [32]. Moreover,  $\gamma\text{-Al}_2\text{O}_3$ , an oxide with both acidic and basic surface sites, is reported to activate  $\text{H}_2\text{O}_2$  and catalyze styrene epoxidation [33] and Au supported on  $\gamma\text{-Al}_2\text{O}_3$  is reported to form  $\text{H}_2\text{O}_2$  from  $\text{H}_2$  and  $\text{O}_2$  at elevated pressures [34]. A theoretical study by Thomson and co-workers showed isolated trimeric Au clusters supported on  $\gamma\text{-Al}_2\text{O}_3$  can be active in the epoxidation of propene with  $\text{H}_2$  and  $\text{O}_2$  [5], but experimental studies on the use of  $\text{Au}/\gamma\text{-Al}_2\text{O}_3$  for propene epoxidation are lacking.



**Scheme 2.** Schematic representation of the activation of  $\text{H}_2\text{O}_2$  on metal oxides such as  $\text{TiO}_2$ , adsorbed  $\text{H}_2\text{O}$  molecules are omitted for clarity.

Interestingly, metal oxides that are readily reduced and re-oxidized catalyze the  $\text{H}_2\text{O}_2$  decomposition reaction.  $\text{MnO}_2$  reacts violently with aqueous  $\text{H}_2\text{O}_2$  involving reduction of  $\text{Mn}^{4+}$  to  $\text{Mn}^{3+}$  and subsequent reoxidation to  $\text{Mn}^{4+}$  in the catalytic mechanism to yield  $\text{H}_2\text{O}$  and  $\text{O}_2$  [35]. Sheldon reported that the readily reducible  $\text{CrO}_3$ , that also has strongly Lewis acidic surface sites, catalyzed the decomposition of peroxide reagents [36].  $\text{TiO}_2$ -based supports are of particular interest, since they show both reducibility of the metal oxide and Lewis acidic surface sites.  $\text{TiO}_2$  is proposed to exist of tetrahedral  $\text{Ti}^{4+}$  species in the case of  $\text{TiO}_2\text{-SiO}_2$  and TS-1. Reduction of these tetrahedral  $\text{Ti}^{4+}$  species yields instable  $\text{Ti}^{3+}$  species that readily oxidize to  $\text{Ti}^{4+}$  in air or  $\text{Ti}^{4+}\text{-OOH}$  species in the presence of peroxides. However, during propene oxidation over  $\text{Au}/\text{TiO}_2\text{-SiO}_2$  catalysts,  $\text{Ti}^{3+}$  is not detected [7,28,37]. In short, metal oxides with Lewis acid sites are proposed to activate  $\text{H}_2\text{O}_2$ , which is a crucial intermediate in the epoxidation reaction.  $\text{H}_2\text{O}_2$  is, however, decomposed by readily reducible metal oxides.

Several individual studies have noticed that some oxides affect the products formed from propene oxidation. This is more extensively studied for supported Ag and Cu catalysts than for supported gold catalysts. Supported Ag and Cu catalysts have been studied using a variety of supports, including  $\alpha\text{-Al}_2\text{O}_3$ ,  $\text{SiO}_2$ ,  $\text{WO}_3$  and  $\text{CaCO}_3$  [32,38–41]. These catalysts often operate at low conversion and low selectivity. Apparently, the acidic supports catalyze the isomerization and total oxidation of PO [42–44]. For supported gold catalysts, the support influence is only reported for  $\text{Au}/\text{TiO}_2$  and  $\text{Au}/\text{TiO}_2\text{-SiO}_2$  catalysts. Au supported on  $\text{TiO}_2$  is reported to deactivate within hours of catalytic testing. The deactivation is proposed to be due to the strong adsorption of PO on Ti-O-Ti sites [45,46]. Dispersed  $\text{TiO}_2$  on  $\text{SiO}_2$  and a TS-1 with low titanium content show no Ti-O-Ti sites. These catalysts possess a high degree of stability [45–48], but PO is reported to adsorb on the epoxidation centers of a  $\text{Au}/\text{TS-1}$  catalyst, thus inhibiting the epoxidation reaction [49]. Acidic  $\text{Ti}^{4+}$  centers of a  $\text{Au}/\text{TiO}_2\text{-SiO}_2$  was shown to catalyze subsequent reactivity

of PO [50]. These reports suggest a contribution of the support acidity on the propene epoxidation reaction, but a systematic study is still missing.

In this study the reactivity of PO over a series of frequently used catalyst supports was examined in the gold-catalyzed propene epoxidation in the presence of H<sub>2</sub> and O<sub>2</sub>. We focus on how physicochemical properties of metal oxides affect the selectivity during propene epoxidation.

## 2. Results and Discussion

### 2.1. Metal Oxide Supported Gold Catalysts

Gold nanoparticles were deposited on metal oxide supports by two different methods: deposition precipitation-urea was performed for the synthesis of Au/TiO<sub>2</sub> and Au/CeO<sub>2</sub>, while the other catalysts were prepared using cation adsorption of Au(en)<sub>2</sub>Cl<sub>3</sub> [15,51–53]. Table 1 lists the structural properties of the supported Au catalysts. Both methods led to Au nanoparticles of 2–5 nm on the metal oxides and quantitative deposition of the gold with a nominal loading of 0.1 wt% for  $\gamma$ -Al<sub>2</sub>O<sub>3</sub> and TiO<sub>2</sub> and 0.2 wt% for SiO<sub>2</sub> and TS-1. The Au/WO<sub>3</sub> and Au/CeO<sub>2</sub> were prepared at a higher gold loading of 1.0 and 2.0 wt%, respectively. No gold particles were observed in the Au/WO<sub>3</sub> catalyst at a lower loading of 0.1%.

**Table 1.** Characteristics of the as prepared Au catalysts supported on different metal oxides.

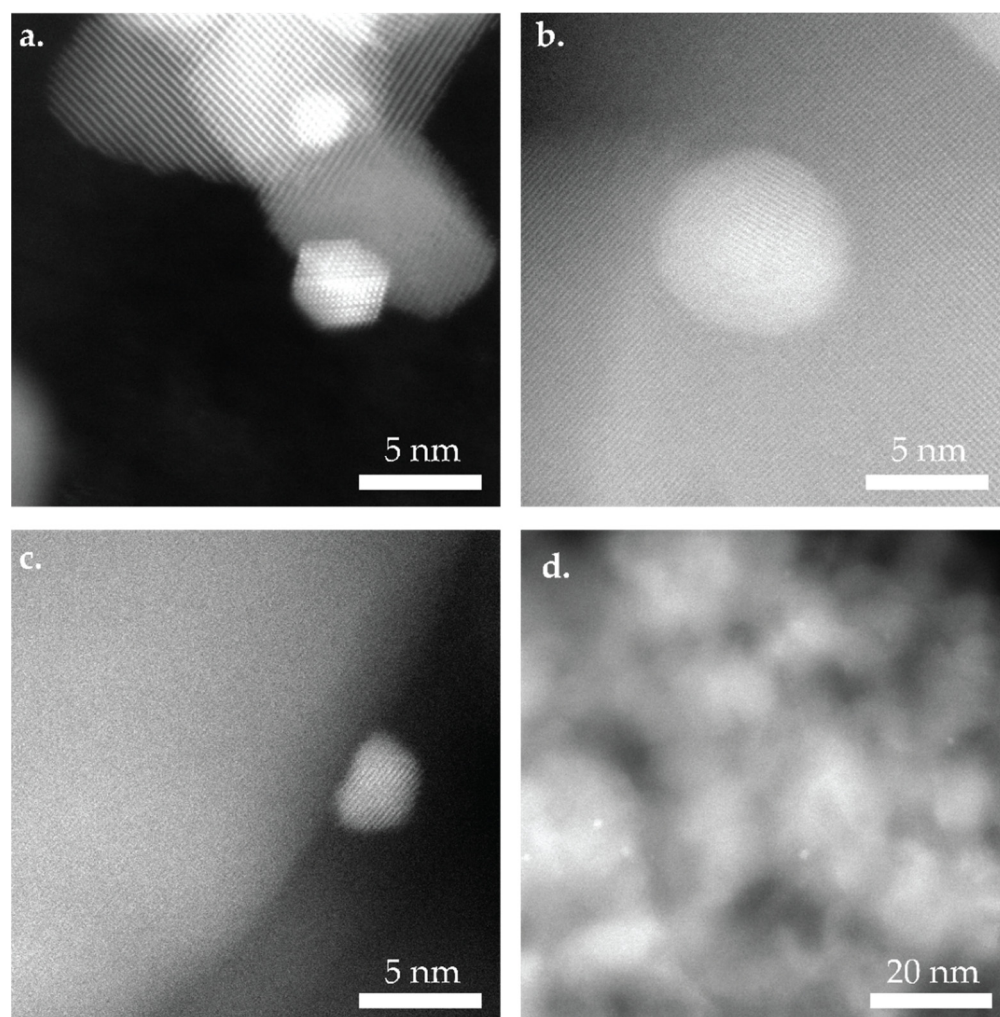
Catalyst	Au Loading (wt%) <sup>a</sup>	Gold Particle Size (nm) <sup>b</sup>	PZC (pH)
Au/CeO <sub>2</sub>	1.89	2.0 ± 0.7	6.2
Au/WO <sub>3</sub>	0.82	5.2 ± 1.5	3.5
Au/TiO <sub>2</sub>	0.10	2.7 ± 0.6	5.5
Au/SiO <sub>2</sub>	0.16	2.3 ± 0.7	6.7
Au/ $\gamma$ -Al <sub>2</sub> O <sub>3</sub>	0.08	n.d.	7.8

n.d. not determined, <sup>a</sup> The gold loading was determined using elemental analysis, <sup>b</sup> number averaged gold particle diameter as derived from transmission electron microscopy.

The acid–base properties of the gold catalysts were studied by means of their point-of-zero-charge (PZC) [27]. The Au/CeO<sub>2</sub> catalyst is amphoteric with a PZC value of 6.2. The Au/WO<sub>3</sub> is acidic with a PZC value of 3.5. The Au/TiO<sub>2</sub> catalyst is mildly acidic with a PZC value of 5.5. The Au/SiO<sub>2</sub> catalyst is amphoteric with a PZC of 6.7. Finally, the Au/ $\gamma$ -Al<sub>2</sub>O<sub>3</sub> is mildly basic with a PZC value of 7.8. The titration curves of the catalysts are included in Figure S1. The observed PZC of the catalysts do not differ much from the pristine supports (Table 2), indicating preservation of the original surface acidity/basicity, except for Au/SiO<sub>2</sub>. The SiO<sub>2</sub> support itself is acidic with a PZC of 4.9, much lower than the final Au/SiO<sub>2</sub> catalyst. This can be explained by the presence of Na<sup>+</sup> from the synthesis, which causes a decrease in the surface acidity [50].

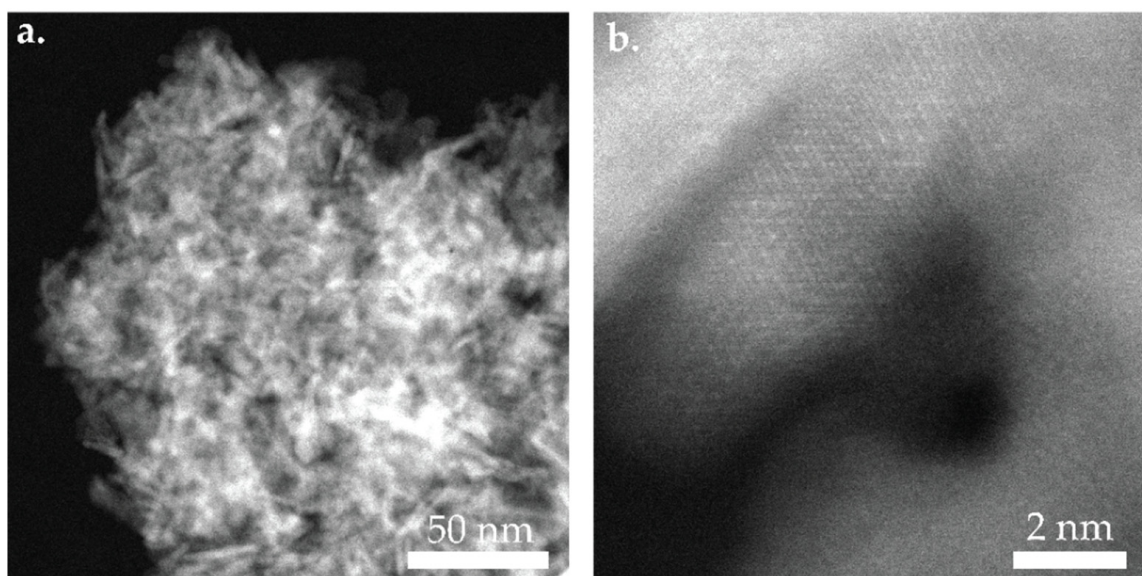
Figure 1 shows representative High-Angle Annular Dark Field Scanning Transmission Electron Microscopy (HAADF-STEM) images of catalysts supported on different metal oxides. The gold particles are visible as bright features on the metal oxide supports. Additional HAADF-STEM images at lower magnification are included as Figures S2 and S3 and show that the gold nanoparticles are homogeneously distributed over the supports. Scanning Electron Microscopy (SEM) images (Figure S4) show the three-dimensional structure of the catalysts and do not show any large gold agglomerates.

Figure 2 shows the HAADF-STEM images of the Au/ $\gamma$ -Al<sub>2</sub>O<sub>3</sub> catalyst at low and high magnification. Elemental analysis confirmed the presence of Au, but almost no nanoparticles with sizes above 2 nm were observed, while according to literature this is the minimum size required for propene epoxidation [9].



**Figure 1.** Representative High-Angle Annular Dark-Field Scanning Transmission Electron Microscopy micrographs of gold nanoparticles supported on oxidic supports. (a) Au/CeO<sub>2</sub>, (b) Au/WO<sub>3</sub>, (c) Au/TiO<sub>2</sub>, (d) Au/SiO<sub>2</sub>.

The supported gold catalysts were tested in propene epoxidation at 200 °C with 10% propene, 10% oxygen and 10% hydrogen in helium at a typical flow of 10,000 mL/g<sub>cat</sub>/h. The pristine support materials did not show any activity under the studied conditions. Figure 3 shows the propene and hydrogen conversions of the different supported gold catalysts. In addition, Table S1 contains a full overview of the conversions and selectivities to the various oxidation products and Table S2 shows a comparison of the catalysts tested in this work with similar catalysts in literature. The highest conversion of up to 17.4% as was observed for the Au/CeO<sub>2</sub> catalyst, the high conversion of propene under oxidative conditions using similar Au/CeO<sub>2</sub> catalysts is well known in literature, for example Louis et al. observed 50% propene conversion at 294 °C. [15] The Au/γ-Al<sub>2</sub>O<sub>3</sub> catalyst showed a propene conversion below 0.1%. While the other catalysts showed propene conversions of up to 0.5%. The Au/γ-Al<sub>2</sub>O<sub>3</sub> catalyst was the least active in the combustion of hydrogen and showed a hydrogen conversion of only 8.9%. The Au/WO<sub>3</sub> and Au/TiO<sub>2</sub> catalysts showed a hydrogen conversion of 27.2% and 34.8%, respectively. The Au/SiO<sub>2</sub> catalyst is more active with a hydrogen conversion of 52.0%, while the Au/CeO<sub>2</sub> catalyst showed a 100% hydrogen conversion. The propene and hydrogen conversions of all catalysts were stable during the catalytic test (Figure S5), with the sole exception of the Au/TiO<sub>2</sub> catalyst which deactivated on-stream (Figures S6 and S7).



**Figure 2.** Representative High-Angle Annular Dark-Field Scanning Transmission Electron Microscopy micrographs of gold nanoparticles supported on  $\gamma$ -Al<sub>2</sub>O<sub>3</sub> (a) at low magnification, (b) at high magnification.

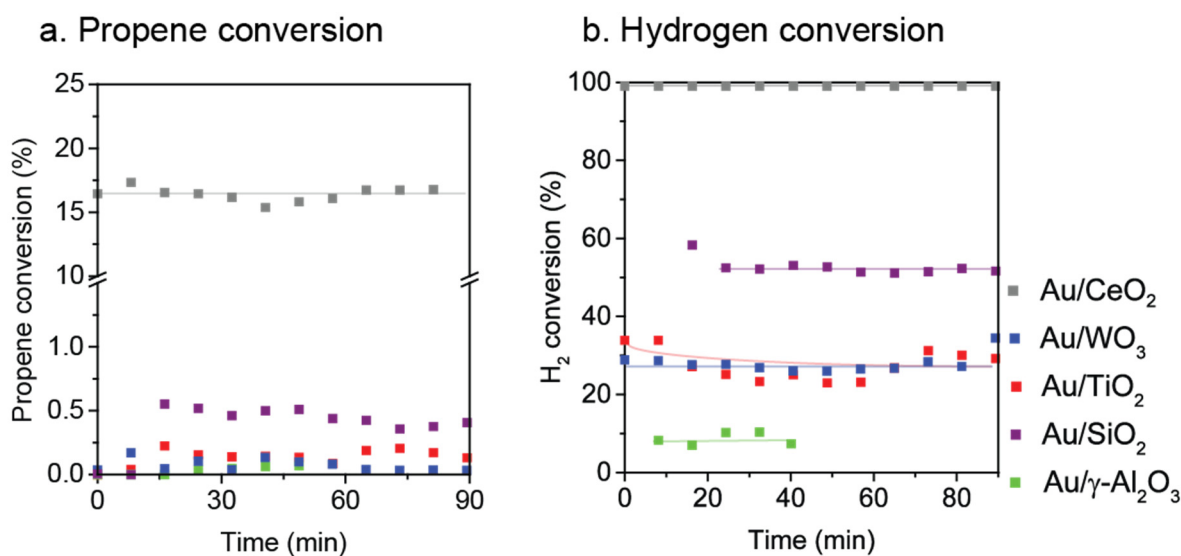


**Figure 3.** Oxidation of propene in the presence of the supported gold catalysts at 200 °C (a) C<sub>3</sub>H<sub>6</sub> conversion, (b) H<sub>2</sub> conversion. Conditions: 150 mg of catalyst, 25 mL/min flow of 10% of each C<sub>3</sub>H<sub>6</sub>, O<sub>2</sub> and H<sub>2</sub> in He. Only 25 mg of catalyst was used in the case of Au/CeO<sub>2</sub>.

Figure 4a presents the activity of the gold catalysts in propene oxidation as function of the gold particle size. The Au/CeO<sub>2</sub> catalyst demonstrated the highest turn-over-frequency (TOF) in propene oxidation of 0.28 s<sup>-1</sup>, defined as molecules of propene converted per surface Au atoms per second [54]. The Au/WO<sub>3</sub> and Au/TiO<sub>2</sub> were almost inactive in propene oxidation; the TOF of the Au/TiO<sub>2</sub> catalyst of 0.01 s<sup>-1</sup> is in agreement with the results of Delgass et al. who observed a TOF of 0.003–0.034 s<sup>-1</sup> for various Au/TiO<sub>2</sub> catalysts at 200 °C [55]. The Au/SiO<sub>2</sub> catalyst shows a TOF of 0.04 s<sup>-1</sup>. The TOF of the Au/ $\gamma$ -Al<sub>2</sub>O<sub>3</sub> catalyst is based on the total amount of Au atoms and is <0.01 s<sup>-1</sup>. The gold catalysts supported on SiO<sub>2</sub> and CeO<sub>2</sub> are the two catalysts with the smallest gold particle size and highest activity in propene and oxidation; however, as discussed in a later section no clear overall relation between Au particle size and activity could be established.

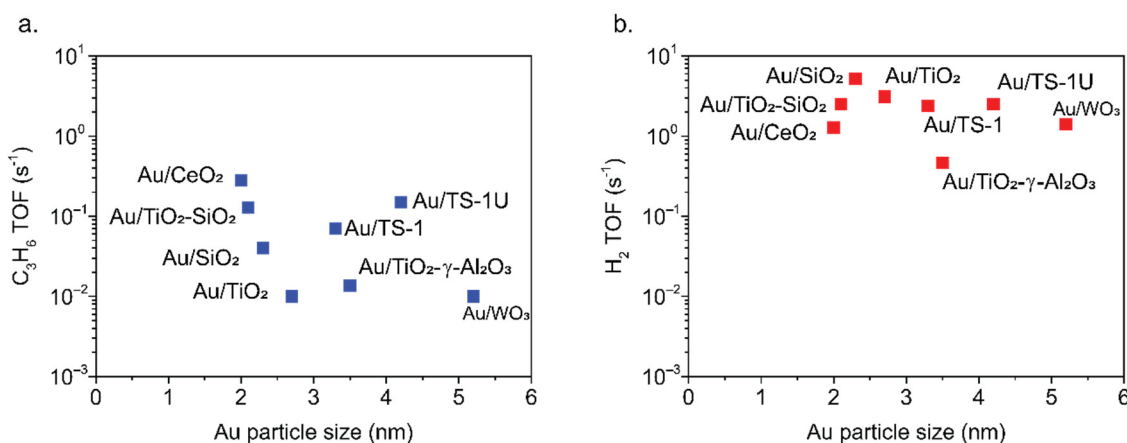


**Figure 4.** Specific activity for the oxidation of propene and the conversion of hydrogen over supported gold catalysts. (a) Activity (TOF) for C<sub>3</sub>H<sub>6</sub> oxidation (b) activity (TOF) for H<sub>2</sub> oxidation. Conditions: 150 mg of catalyst, 10,000 mL/g<sub>cat</sub>/h flow of 10% of each C<sub>3</sub>H<sub>6</sub>, O<sub>2</sub> and H<sub>2</sub> in He at 200 °C. Only 25 mg of catalyst was used in the case of Au/CeO<sub>2</sub>.

The activity of the supported catalysts in H<sub>2</sub> oxidation to H<sub>2</sub>O is given in Figure 4b. The Au/γ-Al<sub>2</sub>O<sub>3</sub> catalyst was almost inactive with a TOF of 0.03 s<sup>-1</sup>. The Au/CeO<sub>2</sub> catalyst showed a TOF of 1.28 s<sup>-1</sup>, defined as molecules of hydrogen converted per surface Au atoms per second. The hydrogen conversion activity increased in the order of Au/WO<sub>3</sub> (1.40 s<sup>-1</sup>), Au/TiO<sub>2</sub> (3.10 s<sup>-1</sup>) and Au/SiO<sub>2</sub> (5.17 s<sup>-1</sup>). For many catalysts, the hydrogen oxidation activity was much higher than the propene oxidation activity and independent of the gold particle size for the studied catalysts. The oxidation of H<sub>2</sub> is generally ascribed to the activation of H<sub>2</sub> and O<sub>2</sub> on the surface of the Au particles primarily forming \*OOH and H<sub>2</sub>O<sub>2</sub> intermediates [56,57]. In the case of Au/TiO<sub>2</sub> catalysts this has been studied in detail. There, a spill-over of the peroxide intermediates to the epoxidation sites at the interface between the Au particle TiO<sub>2</sub> support is proposed to be crucial for PO formation [56,58]. If no-spillover occurs, these peroxide intermediates decompose to form H<sub>2</sub>O, as is predominantly the case for many of the studied catalysts.

The carbon selectivity towards different oxygenates is shown in Figure 5. The Au/CeO<sub>2</sub> catalyst showed 99.8% CO<sub>2</sub> selectivity, with only trace amounts of propanal as side product. This suggests both a strong interaction between gold and the CeO<sub>2</sub> support and readily reducibility of the CeO<sub>2</sub> support [59]. Trace amounts of acetaldehyde from over-oxidation of propene and propanal were formed over the Au/WO<sub>3</sub> catalyst. The Au/TiO<sub>2</sub> produced a mixture of PO (22% selectivity), acetaldehyde and propanal at low activity. The observed mixture of products is most likely due to the relative high reaction temperature of 200 °C compared to literature [37,55] and has been observed by others as well. For example, Nijhuis and co-workers obtained a Au/TiO<sub>2</sub> catalyst that operated at 0.5% conversion and 20% PO selectivity at 90 °C, [37] whereas a higher selectivity was reported at 50 °C of >99% PO. [60] For comparison reasons, we also tested our Au/TiO<sub>2</sub> catalyst at a lower reaction temperature of 100 °C. There our Au/TiO<sub>2</sub> showed a higher selectivity towards PO (Figures S6 and S7), but quickly deactivated as is in accordance with literature [37]. Our Au/SiO<sub>2</sub> is the only catalyst with a high selectivity towards acrolein, this catalyst also shows the formation of trace amounts of PO. Allylic oxidation of propene to acrolein is reported for Au/SiO<sub>2</sub> based catalysts, [60–62] but until now only a single report mentions that Au/SiO<sub>2</sub> can also be active in the epoxidation of propene [63]. The Au/γ-Al<sub>2</sub>O<sub>3</sub> catalyst produced trace amounts of acetone, propanal and acetaldehyde but no PO, which is consistent with previous reports. [62] The Au/SiO<sub>2</sub> and Au/CeO<sub>2</sub> catalysts were also studied in propene oxidation without H<sub>2</sub> at 200 °C. Under those condition, the propene conversion over the Au/SiO<sub>2</sub> catalyst decreased below 0.1% to offer a mixture of acrolein (76%) and acetaldehyde (24%). Interestingly, the Au/CeO<sub>2</sub> showed an increased propene conversion of

22.9%, while the selectivity did not change (99% towards CO<sub>2</sub>), demonstrating the intrinsic differences in catalysis over the Au/CeO<sub>2</sub> and Au/SiO<sub>2</sub> catalysts.

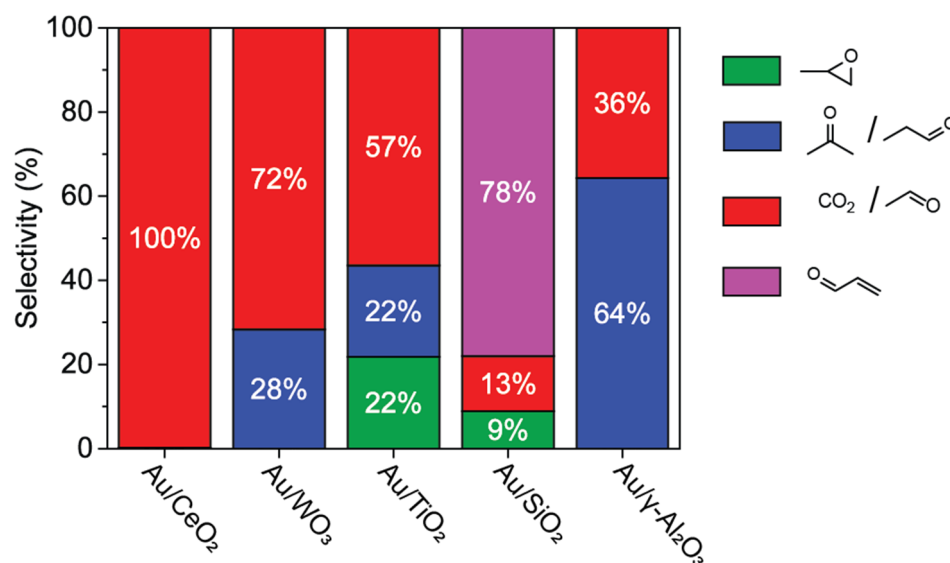


**Figure 5.** Selectivity during the oxidation of propene at 200 °C in the presence of hydrogen over supported gold catalysts. Conditions: 150 mg of catalyst, 10,000 mL/g<sub>cat</sub>/h flow of 10% of each C<sub>3</sub>H<sub>6</sub>, O<sub>2</sub> and H<sub>2</sub> in He at 200 °C. Only 25 mg of catalyst was used in the case of Au/CeO<sub>2</sub>.

If the rate determining step in C<sub>3</sub>H<sub>6</sub> oxidation took place on the gold, a distinct TOF independence of the gold particle size would be expected. However, the observed differences in propene and hydrogen oxidation activity cannot solely be attributed to the varying gold particle sizes. The Au/γ-Al<sub>2</sub>O<sub>3</sub> was the only catalyst that was almost inactive in both propene and hydrogen oxidation. This is most likely due to the absence of 2–5 nm gold nanoparticles. In addition, Au catalysts supported on Al<sub>2</sub>O<sub>3</sub> are often reported to be less active for other reactions, such as butadiene hydrogenation and CO oxidation compared to other supports [64,65]. The high activity of other, such as the Au/WO<sub>3</sub> and Au/TiO<sub>2</sub> catalysts, in H<sub>2</sub> oxidation illustrate that they can generate peroxide intermediates and thus could potentially catalyze propene oxidation. The readily reducible Au/CeO<sub>2</sub> catalyst showed the highest activity in complete oxidation of propene, while the other catalysts showed a mixture of oxygenates. Only the Au/TiO<sub>2</sub> and Au/SiO<sub>2</sub> catalyst show the formation of PO. This clearly stresses the importance of the support acidity/basicity and reducibility for the formation of PO and other oxygenates.

## 2.2. Reactivity of Propene Oxide with Metal Oxide Supports

The influence of the support induced reactivity was studied in more detail by exposing the metal oxide supports to PO and relating the observations to the support reducibility and presence of acidic or basic surface sites.

Figure 6 presents the mass titration curves of the supports, which were used for the determination of their point-of-zero-charge. The physicochemical properties of the different supports are shown in Table 3. Several supports were added to the experiment to clearly show the influence of basicity (CaCO<sub>3</sub>), low surface area and limited surface -OH groups (α-Al<sub>2</sub>O<sub>3</sub>) and Lewis acidity (Titanosilicate-1, TS-1) [66,67]. N<sub>2</sub> physisorption isotherms of the studied supports are included in Figure S8.

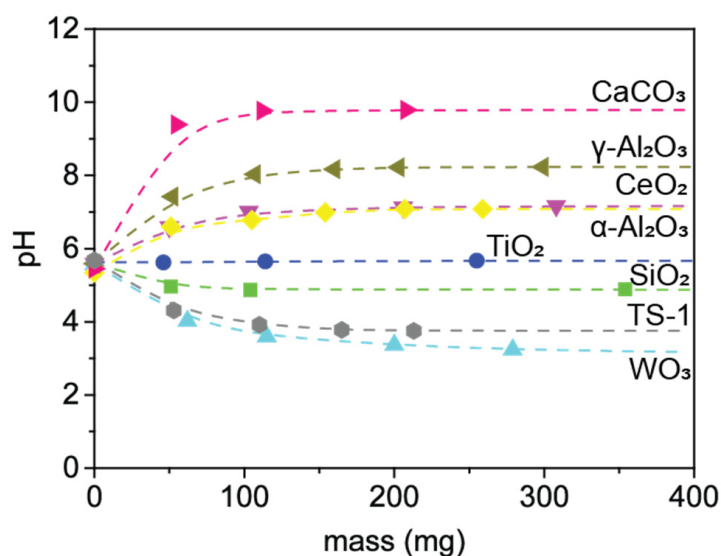


**Figure 6.** Point-of-zero-charge determination of the pristine supports using a 0.1 M KCl solution. Dashed lines were drawn to guide the eye.

The acidity of the metal oxide supports was characterized using infrared spectroscopy with adsorption of pyridine (Py-IR, Figure S9) and temperature programmed desorption of ammonia (NH<sub>3</sub>-TPD, Figure S10) and the results are summarized in Table 2. For the CeO<sub>2</sub> support, Py-IR shows both adsorption of pyridine on Lewis acid (electron accepting) sites as well as oxidation of pyridine to  $\alpha$ -pyridone caused by Ce<sup>4+</sup> to Ce<sup>3+</sup> reduction. [68] Due to the low specific surface area of WO<sub>3</sub> an acid concentration of only 22.3  $\mu\text{mol/g}_{\text{cat}}$  was obtained from NH<sub>3</sub>-TPD with a desorption maximum between 250–400 °C. NH<sub>3</sub>-TPD on TiO<sub>2</sub> shows a 10-fold increase in acid concentration compared to WO<sub>3</sub>, while the acid sites are much weaker with a desorption maximum at 255 °C. Py-IR showed that the TiO<sub>2</sub> consists primarily of Lewis acid sites. TS-1 contains an acid concentration of 82.3  $\mu\text{mol/g}_{\text{cat}}$  based on NH<sub>3</sub> desorption, with a desorption maximum at 201 °C, showing that the acidic sites are weaker than for TiO<sub>2</sub>. Only a minor amount of acid concentration was observed for SiO<sub>2</sub> using NH<sub>3</sub>-TPD, while no acid sites were observed using Py-IR. Although the  $\gamma$ -Al<sub>2</sub>O<sub>3</sub> is basic with a PZC of 8.2 NH<sub>3</sub>-TPD confirms the presence of acid sites with a maximum desorption at 204 °C.

**Table 2.** Overview of the characteristics of the support materials used.

Support	BET S.A. (m <sup>2</sup> /g)	PZC (pH)	-OH Coverage (OH/nm <sup>2</sup> )	Acid Concentration ( $\mu\text{mol/g}_{\text{cat}}$ )
CeO <sub>2</sub>	66	7.2	3.8 [69]	17.7 <sup>a</sup> LA; 0 <sup>a</sup> BA
WO <sub>3</sub>	8	3.1	n.d.	22.3 <sup>b</sup>
TiO <sub>2</sub>	52	5.7	3.3 [70]	239.3 <sup>b</sup>
TS-1	549	3.8	n.d.	111.3 <sup>a</sup> LA; 0.4 <sup>a</sup> BA
SiO <sub>2</sub>	499	4.9	5 [71]	82.3 <sup>b</sup>
$\gamma$ -Al <sub>2</sub> O <sub>3</sub>	249	8.2	8 [72,73]	38.2 <sup>b</sup>
$\alpha$ -Al <sub>2</sub> O <sub>3</sub>	8	7.1	3.5 [74]	0 <sup>a</sup> LA; 0 <sup>a</sup> BA
CaCO <sub>3</sub>	1	9.8	n.d.	385.3 <sup>b</sup>

n.d. not determined, <sup>a</sup> Corresponding to the adsorbed  $\mu\text{mol}$  of pyridine per  $\text{g}_{\text{cat}}$  determined using Py-IR, <sup>LA</sup> Lewis acid, <sup>BA</sup> Brønsted acid, <sup>b</sup> Corresponding to the adsorbed  $\mu\text{mol}$  of NH<sub>3</sub> per  $\text{g}_{\text{cat}}$  determined using NH<sub>3</sub>-TPD.

The pristine supports were tested under reaction conditions (200 °C, 1/1/1/7 ratio of C<sub>3</sub>H<sub>6</sub>/H<sub>2</sub>/O<sub>2</sub>/He at a flow of 10,000 mL/ $\text{g}_{\text{support}}/\text{h}$ ). Without any Au none of the supports showed the formation of propene oxide or other oxygenates. Subsequently,

stacked bed experiments with top to bottom flow were performed with a PO producing Au/TS-1 catalyst on top and the different supports at the bottom. The Au/TS-1 catalyst will be discussed in more detail in the next section. In this way we tested if the observed selectivity was the results of sequential reactions of the PO catalyzed by the supports.

Figure 7 shows the results of the stacked bed experiments. The different support materials are ordered from left to right according to their PZC from acidic to basic. Shown on the far right as a reference is the observed selectivity to the carbon containing products when no extra support was used downstream.

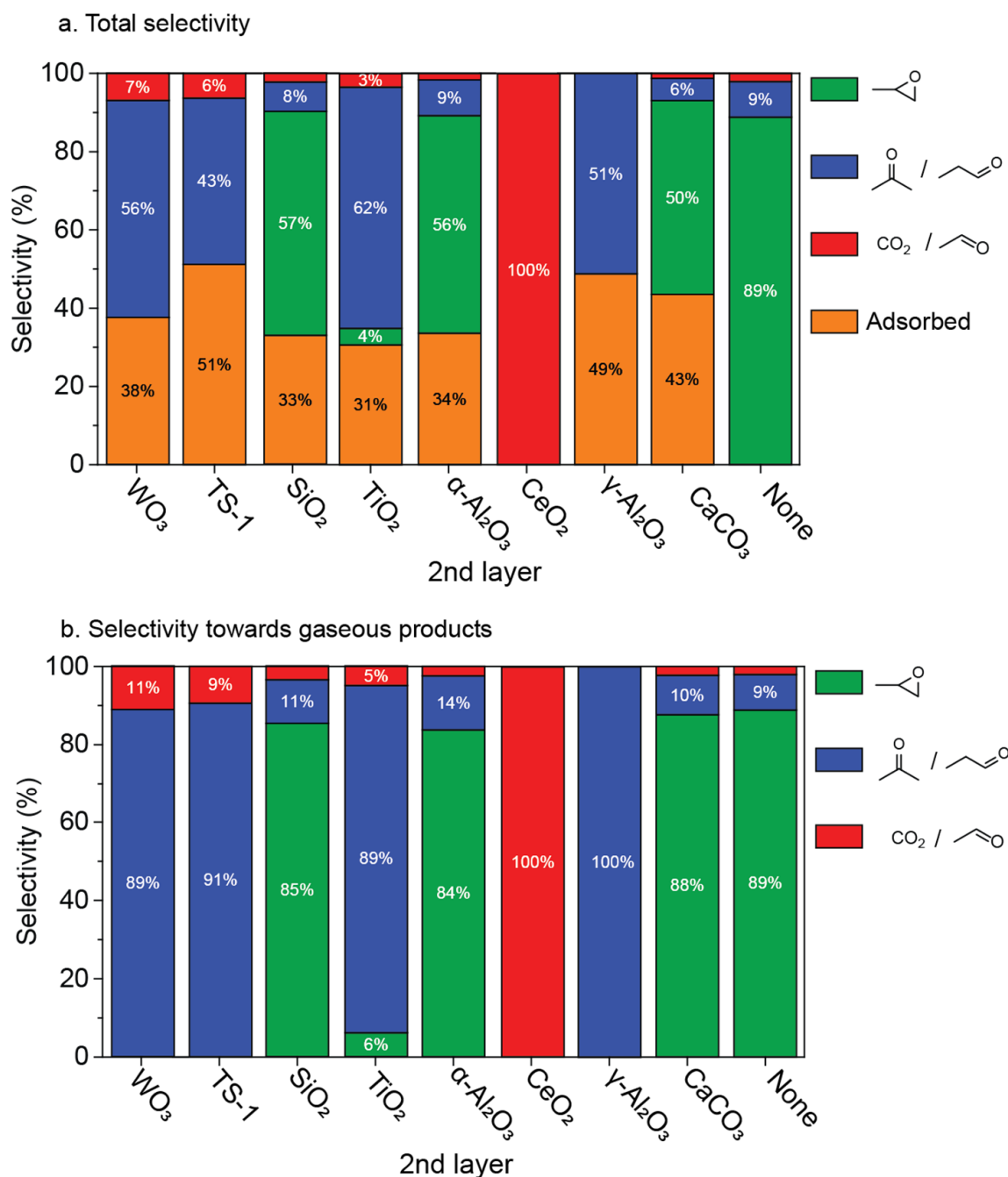


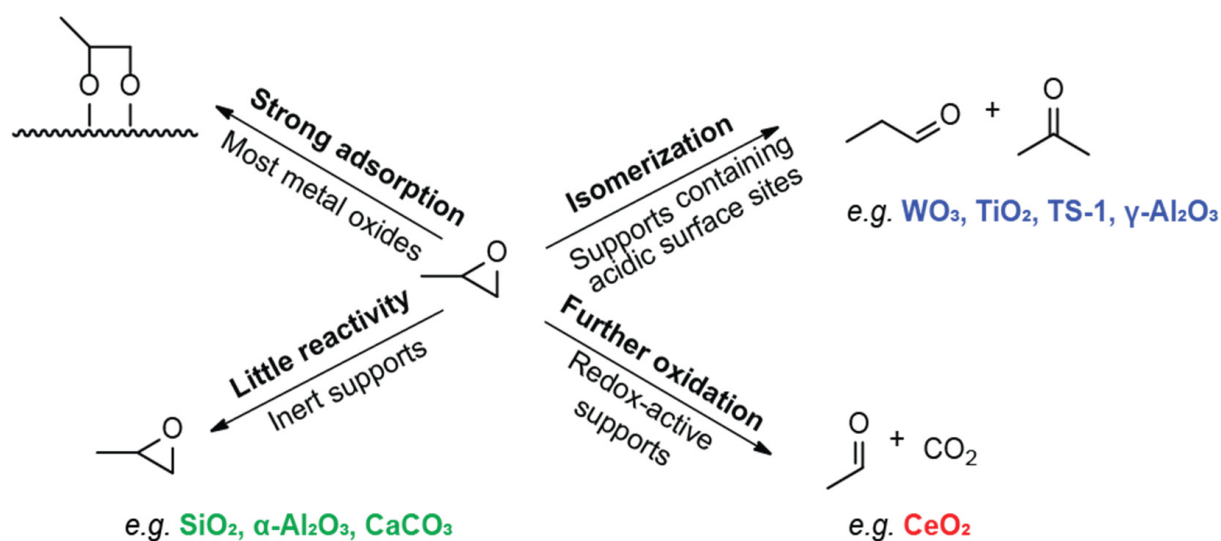
**Figure 7.** Stacked bed experiments where different support materials exposed to a gas feed containing PO. (a) Total selectivity, (b) selectivity towards gaseous products. Conditions: 75 mg of Au/TS-1 catalyst, 150 mg of support material, 10,000 mL/g<sub>support</sub>/h flow of 10% of each C<sub>3</sub>H<sub>6</sub>, O<sub>2</sub> and H<sub>2</sub> in He at 200 °C, the selectivity was the average between 2–3 h of testing.

The carbon mass balance was between 25–50%, hence a large fraction of PO was adsorbed on the support surface during the 2 h of testing (Figure 7a). At prolonged reaction times, the mass balance increased. For example, the  $\alpha$ -Al<sub>2</sub>O<sub>3</sub> shows a carbon mass balance of 50% after two hours of the test, but after 4 h a mass balance of 73% was achieved. This indicates saturation of the specific sites on the support's surface with PO and was also observed for the other supports. For these relative short testing times the selectivity to gaseous products was examined in more detail (Figure 7b).

WO<sub>3</sub>, TS-1, TiO<sub>2</sub> and  $\gamma$ -Al<sub>2</sub>O<sub>3</sub> effectively catalyze the isomerization of PO towards mainly propanal. In addition, WO<sub>3</sub> and TS-1 catalyze the further oxidation of PO towards acetaldehyde. The more inert supports SiO<sub>2</sub>,  $\alpha$ -Al<sub>2</sub>O<sub>3</sub> and CaCO<sub>3</sub> hardly influenced the original product distribution compared to the Au/TS-1 catalyst, except for some adsorption on the surface. The CeO<sub>2</sub> support is unique in catalyzing the complete combustion of the original products towards CO<sub>2</sub>.

The adsorption of PO over TiO<sub>2</sub> and TiO<sub>2</sub>-SiO<sub>2</sub> supported Au catalysts has been reported in literature. Mul and co-workers showed that the adsorption of PO on Au/TiO<sub>2</sub> and Au/TiO<sub>2</sub>-SiO<sub>2</sub> catalysts leads to ring opening of the epoxide and irreversible adsorption of the formed propoxy-species on the TiO<sub>2</sub> sites of the support [45,46]. This is generally accepted to cause deactivation of Au/TiO<sub>2</sub> catalysts, but a comprehensive overview of the reactivity of PO with various metal oxides has not yet been reported.

Scheme 3 illustrates the different types of supports and their reactivity with PO. Neither the PZC of the support nor its specific surface area are very influential factors. The redox active supports (CeO<sub>2</sub>, WO<sub>3</sub> and TiO<sub>2</sub>) [18,75], cause further oxidation of PO to acetaldehyde and at the end complete combustion of PO to CO<sub>2</sub>. This is especially pronounced for CeO<sub>2</sub>, the Au/CeO<sub>2</sub> catalyst was active in the complete oxidation of propene to CO<sub>2</sub> at 19.7% conversion.



**Scheme 3.** Schematic overview of propene oxide reactivity pathways.

The metal oxide supports that possess Brønsted acidic (WO<sub>3</sub>) or Lewis acidic (TS-1, TiO<sub>2</sub>) surface sites [25,76] show isomerization of PO towards propanal and are an example of the heterogeneously catalyzed Meinwald rearrangement [51,77]. The isomerization over basic  $\gamma$ -Al<sub>2</sub>O<sub>3</sub> towards acetone and propanal is facilitated by either basic surface sites or Lewis acidic surface sites that are present at surface defects. The presence of these acidic sites was confirmed by NH<sub>3</sub>-TPD.

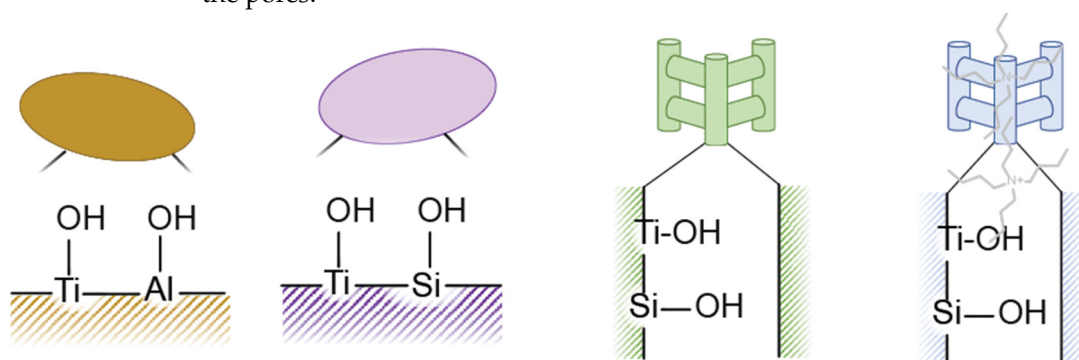
Whereas the metal oxides that contain acidic surface sites show isomerization of the desired PO, the oxide supports that lack acidic surface sites, such as SiO<sub>2</sub> and CaCO<sub>3</sub>, show higher PO selectivity. Factors that are beneficial to prevent sequential reactions of the PO once it has been formed are an inert surface as observed for the SiO<sub>2</sub> support, a low specific

surface area as for the  $\text{CaCO}_3$  support and a low density of surface -OH groups as for the  $\alpha\text{-Al}_2\text{O}_3$  support

### 2.3. Au Supported on $\text{Ti}^{4+}$ Modified Oxides

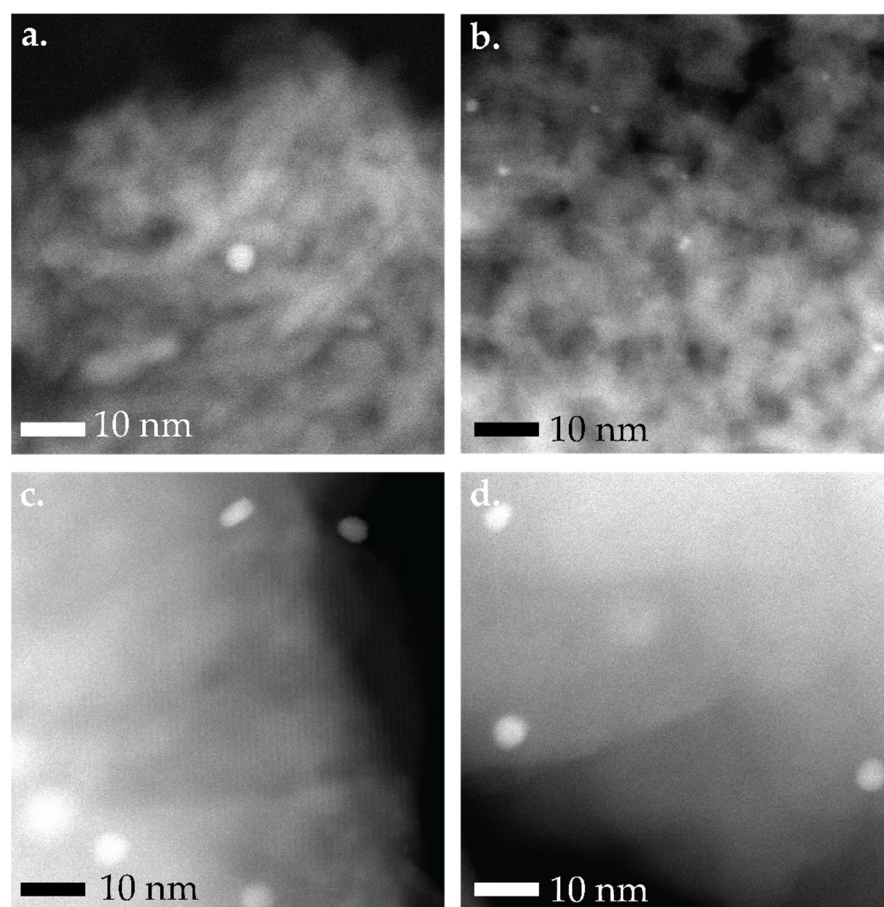
Until now it has become clear that three important conditions have to be fulfilled simultaneously by a good supported Au catalyst for propene epoxidation: peroxide species should be formed (as is true for almost all supports tested), these species should be able to spill over to the site at which propene is adsorbed (which strongly depends on the Au-support interface) and the support itself should not cause sequential reaction of the propene oxide. Most active and selective gold catalysts for propene epoxidation are often based on TS-1 as support [78,79]. However, as evidenced above, the TS-1 support can catalyze isomerization of PO towards propanal, which is often reported as a side product in propene epoxidation using Au/TS-1 catalysts. Here we compare the activity and selectivity of Au supported on various  $\text{TiO}_2$  containing supports in propene epoxidation.

Figure 8 shows a schematic representation of the various  $\text{TiO}_2$ -supports:  $\text{TiO}_2$  grafted on  $\gamma\text{-Al}_2\text{O}_3$  ( $\text{TiO}_2\text{-}\gamma\text{-Al}_2\text{O}_3$ ),  $\text{TiO}_2$  grafted on  $\text{SiO}_2$  ( $\text{TiO}_2\text{-SiO}_2$ ) and two types of TS-1, which differ in having accessible pores (TS-1) or blocked pores (TS-1U). Gold nanoparticles were deposited on  $\text{TiO}_2\text{-}\gamma\text{-Al}_2\text{O}_3$ ,  $\text{TiO}_2\text{-SiO}_2$  and the two types of TS-1 by cation adsorption of  $\text{Au}(\text{en})_2\text{Cl}_3$  with  $\text{Na}_2\text{CO}_3$  for pH control at a nominal loading of 0.20 wt% for Au/TS-1 and normalized to the specific surface area of the other supports. For the Au/TS-1 catalyst, the template directing reagents were removed prior to gold deposition, gold deposition thus took place in the pores as well as on the surface of the TS-1 crystals. On the contrary, for the Au/TS-1U catalyst, the template directing reagents were removed only after gold deposition, hence gold was present on the surface of the TS-1U crystals rather than in the pores.



**Figure 8.** Schematic representation of (from left to right)  $\text{TiO}_2\text{-}\gamma\text{-Al}_2\text{O}_3$ ,  $\text{TiO}_2\text{-SiO}_2$ , TS-1 and TS-1U.

Shown in Figure 9 are representative Bright-Field TEM (BF TEM) and HAADF-STEM images of the gold catalysts supported on different  $\text{TiO}_2$ -based supports. The gold particles are typically between 1.5–4.2 nm in size. Table 3 summarizes the structural properties of the Au catalysts. The PZC of the Ti-modified supports was lower than for pristine  $\gamma\text{-Al}_2\text{O}_3$  and  $\text{SiO}_2$  (Table 2), which is indicative for the formation of acidic tetrahedral  $\text{Ti}^{4+}$  sites on the supports [45,80]. The absence of oligomeric  $\text{TiO}_2$ , which is detrimental for propene epoxidation, was confirmed by diffuse reflectance UV-Vis (Figure S11). Upon gold deposition, the PZC typically increased to 6.7–7.7, indicating that  $\text{Na}^+$  was present and neutralized the acidic  $\text{Ti}^{4+}$  sites. The presence of  $\text{Na}^+$  was confirmed by Elemental Dispersive X-ray spectroscopy (Figure S3), but  $\text{NH}_3\text{-TPD}$  shows no change in acid concentration between TS-1 ( $82.3 \mu\text{mol}_{\text{NH}_3}/\text{g}$ ) and Au/TS-1 ( $87.6 \mu\text{mol}_{\text{NH}_3}/\text{g}$ ) (Figure S10), although their strength is slightly lower with a desorption maximum at  $196^\circ\text{C}$  vs.  $201^\circ\text{C}$ . Only in the case of Au/TS-1U the PZC of the final catalyst does not differ from the TS-1 support. There, the template directing reactants blocked the micropores and  $\text{Na}^+$  did thus not neutralize the acidic  $\text{Ti}^{4+}$  sites in the micropores.



**Figure 9.** Representative HAADF-STEM images of (a) Au/TiO<sub>2</sub>-γ-Al<sub>2</sub>O<sub>3</sub>, (b) Au/TiO<sub>2</sub>-SiO<sub>2</sub>, (c) Au/TS-1, (d) Au/TS-1U.

**Table 3.** Characteristics of the as prepared Au catalysts.

Catalyst.	Au Loading (wt%) <sup>a</sup>	Gold Particle Size (nm) <sup>b</sup>	PZC TiO <sub>2</sub> -Support (pH)	PZC Catalyst (pH)
Au/TiO <sub>2</sub> -γ-Al <sub>2</sub> O <sub>3</sub>	0.08	3.5 ± 0.5	6.0	7.7
Au/TiO <sub>2</sub> -SiO <sub>2</sub>	0.16	2.1 ± 0.7	2.9	6.8
Au/TS-1	0.19	3.3 ± 1.0	3.8	6.7
Au/TS-1U	0.22	4.2 ± 1.1	3.8 <sup>c</sup>	3.8

<sup>a</sup> The gold loading was determined using elemental analysis, <sup>b</sup> number averaged gold particle size, <sup>c</sup> the PZC of TS-1.

The supported gold catalysts were tested in propene epoxidation at 200 °C with 10% propene, 10% oxygen and 10% hydrogen in helium at a flow of 10,000 mL/g<sub>cat</sub>/h. Figure 10 shows the propene and hydrogen conversions, while the selectivity to the various oxygenates is shown in Figure 11 and Table S1 contains a full overview of the conversions and selectivities and Table S2 contains a comparison with catalysts reported in literature. The gold catalyst supported on TiO<sub>2</sub>-γ-Al<sub>2</sub>O<sub>3</sub> showed the lowest propene and hydrogen conversion, of, respectively, 0.5% and 21.9%. Like the Au/γ-Al<sub>2</sub>O<sub>3</sub> catalyst, the Au/TiO<sub>2</sub>-γ-Al<sub>2</sub>O<sub>3</sub> catalyst showed the formation of trace amounts of oxygenates. The gold catalyst supported on TiO<sub>2</sub>-SiO<sub>2</sub> showed the highest propene and hydrogen conversion of, respectively, 3.6% and 78.8%, although this catalyst slightly deactivated during the catalytic test. The Au-TiO<sub>2</sub>-SiO<sub>2</sub> catalyst showed an initial propene conversion of 4.7% which decreased to 3.6 after 90 min (a loss of 24% of activity). The deactivation of PO producing Au/TiO<sub>2</sub>-SiO<sub>2</sub> catalysts is well reported in literature, Haruta et al. showed a deactivation of the propene conversion of 20–30% within 1.5 h over Au/Ti-MCM-41 catalysts. [47] A similar catalyst is

reported in literature and studied under the same conditions, there a propene conversion of 1.9% was obtained. [81] The catalysts supported on TS-1 and TS-1U showed a stable propene conversion of 1.7% and 3.0%, respectively, with a hydrogen conversion at 60.5% and 59.2%. The Au/TS-1 catalyst did not show any deactivation during the catalytic test, while the Au/TS-1U showed a deactivation of the propene conversion from 3.2% to 3.0% during the catalytic test. Hence the performance was clearly somewhat better for the TS-1U than for TS-1. The H<sub>2</sub> conversion of all the catalyst was stable during the 1.5 h catalytic test. Compared to literature, Lu and co-workers attempted to deposit Au on uncalcined and calcined TS-1, but due to the low PZC of calcined TS-1 were not able to deposit < 5 nm Au particles on this support. Hence their catalyst was nearly inactive under the studied conditions. [82] Delgass et al. report Au/TS-1 catalysts operating at 2.0–3.5% propene conversion and 3.5–18.9% H<sub>2</sub> conversion (14,000 mL/g<sub>cat</sub>/h flow of 10% of each reactant in N<sub>2</sub> at 200–205 °C). The much higher H<sub>2</sub> conversion in our results is likely due to the low Au loading used by Delgass of 0.01 up to 0.09 wt% compared to the 0.22 wt% in our work [83].

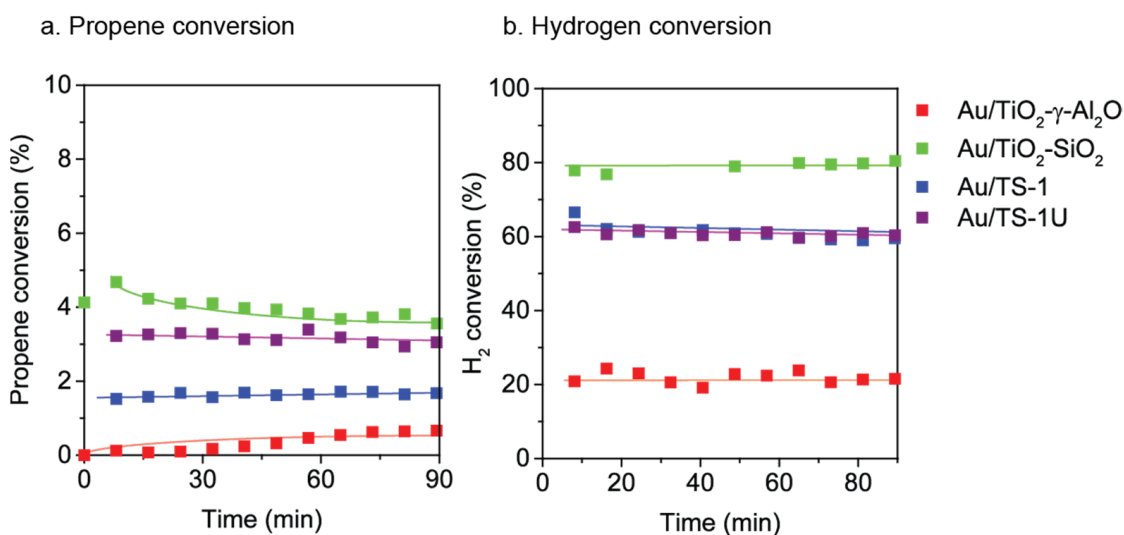


**Figure 10.** Conversion during propene (a) and hydrogen (b) oxidation over gold catalysts supported on Ti<sup>4+</sup>-modified materials. Conditions: 150 mg of catalyst, 10,000 mL/g<sub>cat</sub>/h flow of 10% of each C<sub>3</sub>H<sub>6</sub>, O<sub>2</sub> and H<sub>2</sub> in He at 200 °C.

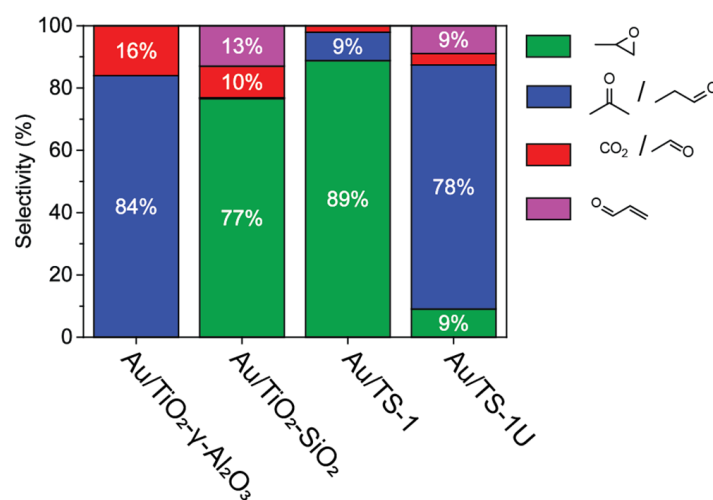


**Figure 11.** Carbon selectivity during the oxidation of propene over gold on Ti-modified supports. Conditions: 150 mg of catalyst, 10,000 mL/g<sub>cat</sub>/h flow of 10% of each C<sub>3</sub>H<sub>6</sub>, O<sub>2</sub> and H<sub>2</sub> in He at 200 °C.

Figure 11 shows the selectivity to the various oxygenates. The Au/TiO<sub>2</sub>- $\gamma$ -Al<sub>2</sub>O<sub>3</sub> did not produce a significant amount of PO and formed only trace amounts of acetone and propanal. The Au/TiO<sub>2</sub>-SiO<sub>2</sub> and Au/TS-1 catalyst both have a high activity and selectivity towards PO, which is in accordance with reports in literature where similar catalysts show >83% selectivity towards PO [81,83]. While Ba(NO<sub>3</sub>)<sub>2</sub> promoted and silylated Au/TiO<sub>2</sub>-SiO<sub>2</sub> catalysts an increased activity and selectivity towards PO formation. [84] Figure 12 shows the TOF for PO formation, which was 0.06 s<sup>-1</sup> for the Au/TS-1 catalyst (0.07 s<sup>-1</sup> for propene oxidation) with an average gold Au particles size of 3.3 nm, in line with literature in which Delgass et al. reported a TOF of ca. 0.06 s<sup>-1</sup> for 3.4 nm gold particles supported on TS-1 [54]. Remarkably the Au/TS-1U catalysts showed a much higher propene oxidation activity (TOF 0.15 s<sup>-1</sup>), but only 9% selectivity towards PO. Instead, this catalyst showed a high selectivity towards propanal, which is probably the result of subsequent PO isomerization, as evidenced from the stacked bed experiments discussed earlier. This is in accordance with previous results by Haruta et al. who showed that an extensively washed Au/TS-1 catalyst show 3% selectivity towards PO and 74% selectivity towards propanal [60]. A preliminary attempt to impregnate the Au/TS-1U catalyst with NaNO<sub>3</sub> or Ba(NO<sub>3</sub>)<sub>2</sub> to inhibit the isomerization reaction did not significantly change the activity or selectivity of the catalyst. These results clearly show that Ti<sup>4+</sup>-based supports such as TiO<sub>2</sub>-SiO<sub>2</sub> and TS-1 are crucial for the epoxidation of propene, it highlights the promoting effect of Na<sup>+</sup> for the propene epoxidation, and it also shows that other catalysts do show higher peroxide formation rates, and are limited by subsequent reactions of the propene oxide that is formed, hence showing the way to further improvement of these propene epoxidation catalysts.

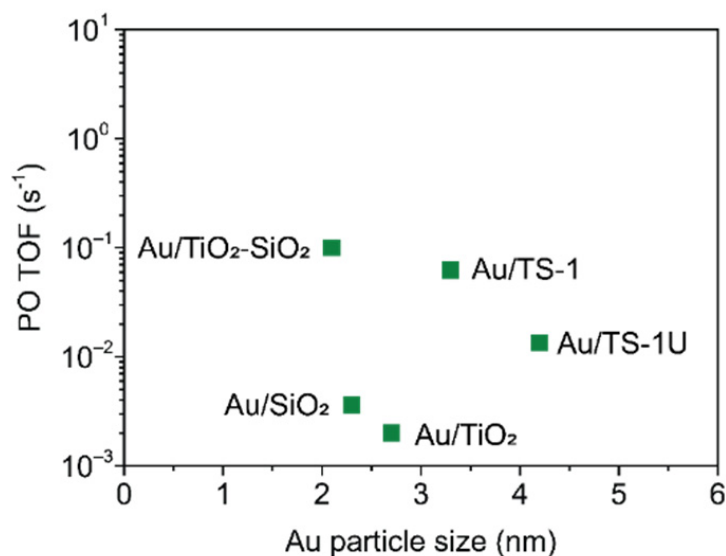


**Figure 12.** Activity for the formation of propene oxide (PO) in the presence of H<sub>2</sub> and O<sub>2</sub> over gold catalysts supported on Ti<sup>4+</sup>-modified oxides, TiO<sub>2</sub> and SiO<sub>2</sub>. Conditions: 150 mg of catalyst, 10,000 mL/g<sub>cat</sub>/h flow of 10% of each C<sub>3</sub>H<sub>6</sub>, O<sub>2</sub> and H<sub>2</sub> in He at 200 °C.

### 3. Materials and Methods

#### 3.1. Materials

SiO<sub>2</sub> (GRACE<sup>®</sup> Davicat SI 1404) was kindly provided by GRACE, Columbia, MD, USA. CeO<sub>2</sub> (nanopowder, 99.5% min, Alfa Aesar, Haverhill, MA, USA), TiO<sub>2</sub> (P25, Evonik, Essen, Germany), WO<sub>3</sub> (nanopowder, Sigma-Aldrich, Amsterdam, The Netherlands),  $\gamma$ -Al<sub>2</sub>O<sub>3</sub> (gamma-phase, Alfa Aesar, Haverhill, MA, USA),  $\alpha$ -Al<sub>2</sub>O<sub>3</sub> (BASF), CaCO<sub>3</sub> (99.95%, Sigma-Aldrich, Amsterdam, The Netherlands), HAuCl<sub>4</sub>·3H<sub>2</sub>O (ACS reagent,  $\geq$ 49.0% Au, ACROS Organics, Geel, Belgium), Na<sub>2</sub>CO<sub>3</sub> ( $\geq$ 99.5%, Sigma-Aldrich, Amsterdam, The Netherlands), NaNO<sub>3</sub> ( $\geq$ 99.0%, Sigma-Aldrich, Amsterdam, The Netherlands), Ba(NO<sub>3</sub>)<sub>2</sub> (ACS Reagent, >99.0%, Sigma-Aldrich, Amsterdam, The Netherlands), NaBH<sub>4</sub> (Reagent-

Plus, 99%, Sigma-Aldrich, Amsterdam, The Netherlands), KCl ( $\geq 99\%$ , Fisher Chemical, Pittsburgh, PA, USA), AgNO<sub>3</sub> ( $\geq 99.0\%$ , Sigma-Aldrich, Amsterdam, The Netherlands), TiCp<sub>2</sub>Cl<sub>2</sub> (99+%, STREM, Newburyport, MA, USA), Ti(OBu)<sub>4</sub> ( $\geq 97\%$ , Fluka Chemie, Buchs, Switzerland), Tween<sup>®</sup> 20 (Polyethylene glycol sorbitan monolaurate, for synthesis, Sigma-Aldrich, Amsterdam, The Netherlands), tetrapropyl ammonium hydroxide (TPAOH, 25% in H<sub>2</sub>O, Sigma-Aldrich, Amsterdam, The Netherlands), tetraethyl orthosilicate (98%, ACROS Organics, Geel, Belgium), isopropanol (99+%, ACROS Organics, Geel, Belgium), ethanol (99.5%, extra dry, ACROS Organics, Geel, Belgium), urea (ACS Reagent, Sigma-Aldrich, Amsterdam, The Netherlands), chloroform (anhydrous, 99.9%, ACROS Organics, Geel, Belgium), 1,2-dichloroethane (anhydrous, 99.8%, ACROS Organics, Geel, Belgium), triethylamine (anhydrous,  $\geq 99.5\%$ , Sigma-Aldrich, Amsterdam, The Netherlands) and ethylenediamine (99.5%, Sigma-Aldrich, Amsterdam, The Netherlands) were purchased from the indicated providers and used without further purification.

### 3.2. General Considerations

All manipulations involving gold were performed in the absence of light in glassware that was rinsed with aqua regia prior to use. After preparation the supported gold catalysts were stored in the absence of light in an exicator under Ar. For inert manipulations, common Schlenk techniques and equipment were used under N<sub>2</sub> using glassware with Teflon joints.

#### 3.2.1. Support Preparation: Titanosilicate-1

Following a literature procedure [85], 2.00 g Tween<sup>®</sup> 20 was dissolved in 26.40 g Milli-Q water and added to 24.60 g of a 25% tetrapropyl ammonium hydroxide solution in water. An amount of 36.06 g of tetraethyl orthosilicate was added under vigorous stirring. After addition stirring was continued for 1 h. Subsequently 1.81 g of tetrabutyl orthotitanate in 10 mL isopropanol was added dropwise. After 1 h of stirring, the mixture was transferred to a 250 mL Teflon lined autoclave (Berghof) and heated to 160 °C for 18 h under autogenous pressure. The TS-1 was retrieved via centrifugation (6000 rpm, 10 min) and dried under ambient conditions. The crude and uncalcined TS-1 is denoted as TS-1U. An amount of 10.90 g of the crude TS-1 was calcined at 550 °C for 6 h under a flow of compressed air at a ramp of 5 °C/min to offer calcined TS-1 as a white powder, denoted as TS-1.

#### 3.2.2. Support Preparation: TiO<sub>2</sub>-SiO<sub>2</sub> and TiO<sub>2</sub>- $\gamma$ -Al<sub>2</sub>O<sub>3</sub>

Following an adapted literature procedure [86], 1.5 g of dried support (SiO<sub>2</sub> or  $\gamma$ -Al<sub>2</sub>O<sub>3</sub>) was dispersed in 30 mL anhydrous dichloroethane under an N<sub>2</sub> atmosphere followed by the slow addition of an appropriate amount of TiCp<sub>2</sub>Cl<sub>2</sub> in 50 mL anhydrous dichloroethane. The red mixture was heated to 60 °C for 1 h under stirring. Subsequently 0.50 mL anhydrous NEt<sub>3</sub> was added to induce the grafting. Heating at 60 °C was continued for 3.5 h. After cooling to room temperature, the solids were collected via filtration and washed three times with 10 mL anhydrous chloroform. The powder was dried under vacuum and calcined under static air at 500 °C for 4 h with a ramp of 10 °C/min to offer the TiO<sub>2</sub>-functionalized supports as a white powder.

#### 3.2.3. Bis(ethylenediamine) Gold (III) Chloride

Following an adapted literature procedure [87], 0.15 mL of ethylene diamine was added dropwise under vigorous stirring, to a yellow solution of tetrachloroauric acid hydrate (0.31 g in 1 mL Milli-Q water). Twenty milliliters of ethanol was added immediately to precipitate Au(en)<sub>2</sub>Cl<sub>3</sub>. The crude product was washed with plenty of ethanol and diethyl ether and dried in the dark at ambient conditions to offer 0.19 g of Au(en)<sub>2</sub>Cl<sub>3</sub> as a beige powder.

### 3.2.4. Catalyst Preparation: Deposition Precipitation Urea

The Au/CeO<sub>2</sub> and Au/TiO<sub>2</sub> catalysts were prepared following the literature procedure by Louis et al. [15,65].

### 3.2.5. Catalyst Preparation: Cation Adsorption of Au(en)<sub>2</sub>Cl<sub>3</sub>

One gram of support (SiO<sub>2</sub>, WO<sub>3</sub>,  $\gamma$ -Al<sub>2</sub>O<sub>3</sub> or TS-1U) was dispersed in 50 mL Milli-Q water and an appropriate amount of Au(en)<sub>2</sub>Cl<sub>3</sub> in 10 mL Milli-Q water was added under vigorous stirring. (In the case of TS-1, 5.0 g support was dispersed in 250 mL Milli-Q water). Subsequently the pH was raised to 9.0–9.5 by dropwise addition of a 5 wt% Na<sub>2</sub>CO<sub>3</sub> solution in Milli-Q water. The mixture was allowed to stir for three hours. The solids were collected via centrifugation (7000 rpm, 10 min) and washed three times with plenty of Milli-Q water, with centrifugation in between (7000 rpm, 10 min). The solids were allowed to dry at room temperature in the dark and subsequently reduced at 300 °C for 2 h (30% H<sub>2</sub> in N<sub>2</sub>, 5 °C/min, 80 mL/min) and calcined at 450 °C for 3 h (20% O<sub>2</sub> in N<sub>2</sub>, 5 °C/min, 80 mL/min) to offer the Au catalysts as pink to purple colored powders. Adsorption of Au(en)<sub>2</sub>Cl<sub>3</sub> was confirmed by addition of NaBH<sub>4</sub> to the supernatant liquid of the first washings, no Au precipitate was formed. Removal of Cl<sup>-</sup> was confirmed by adding AgNO<sub>3</sub> to the supernatant liquid of the last washing step: no AgCl precipitate was formed.

### 3.2.6. Post Synthesis Treatment of Au/TS-1U

An amount of 0.25 g of previously synthesized Au/TS-1U was dispersed in 10 mL Milli-Q water. One milliliter of a 3.5 mM NaNO<sub>3</sub> or Ba(NO<sub>3</sub>)<sub>2</sub> solution was added dropwise and the resulting dispersion was stirred in the dark for 2 h. Subsequently the water was removed in vacuo. The resulting catalysts were dried in the dark under vacuum at room temperature.

## 3.3. Catalyst Characterization

Elemental analysis was performed using inductively coupled plasmon mass spectrometer at the Mikroanalytisches Labor Kolbe, Germany. Bright Field Transmission Electron Microscopy (TEM) images were collected on Talos L120. High-Angle Annular Dark Field Scanning Transmission Electron Microscopy (HAADF-STEM) images were collected on a Talos F200X. Typically 100–200 individual particles were counted for the determination of the average particle size, for Au/WO<sub>3</sub> only 50–100 particles were observed in 10+ images, for Au/ $\gamma$ -Al<sub>2</sub>O<sub>3</sub> and Au/TiO<sub>2</sub>- $\gamma$ -Al<sub>2</sub>O<sub>3</sub> < 10 particles were observed in 20+ images. Double aberration corrected HAADF-STEM images were collected on a Spectra 300, operating at 300 kV. For the EM images the samples were prepared by drop casting from ethanolic dispersion on lacey carbon Cu grids.

The weight loss of the catalysts was determined using a PerkinElmer TGA 8000 equipped with a mass spectrometer (MS) under 20% O<sub>2</sub> in Ar at 14 mL/min total flow. Diffuse reflectance UV-Vis was recorded under ambient conditions on a Perkin Elmer Lambda 950S coupled with a 150 mm integrating sphere and an InGaAs detector, using BaSO<sub>4</sub> as reference (200–800 nm, 4 nm interval, slit size 4 nm). The point-of-zero-charges of the samples were determined using mass titrations. The supports were suspended in 3.000 mL of a 0.1 M KCl solution in Milli-Q water and equilibrated. The pH of the solution was measured using a Radiometer analytical MeterLab PHM210 standard pH meter. Nitrogen physisorption measurements were performed at 77 K using a Micromeritics TriStar 3000.

Fourier-Transform Infrared Spectroscopy with temperature programmed pyridine adsorption and desorption (FTIR) was performed on a ThermoScientific Nicolet iS5 using a custom-built cell in transmission mode. Sixty-four scans were used for the background, 32 scans for samples at a resolution of 4 cm<sup>-1</sup>. In brief, self-supporting pellets of approximately 20 mg (12 mm diameter) were evacuated in vacuo at 200 °C for 1 h, ramp 10 °C/min, followed by cooling to 30 °C. At 30 °C 15 mbar of pyridine (Sigma-Aldrich, 99.8%) vapor was introduced and allowed to adsorb on the sample for 30 min, with spectra collected every 5 min. After 30 min the sample was evacuated for 15 min under a dynamic

high vacuum. Followed by temperature programmed desorption of the pyridine under dynamic high vacuum (30–500 °C, ramp 5 °C/min) with spectra recorded every 25 °C. Pyridine adsorbed on Lewis acid sites were characterized by vibrations of coordinated pyridine at 1600–1605, 1575, 1490 and 1445 cm<sup>-1</sup>, respectively, due to the ν<sub>8a</sub>, ν<sub>8b</sub>, ν<sub>19a</sub> and ν<sub>19b</sub> vibrations of the pyridine molecule. Brønsted acid sites were observed for TiO<sub>2</sub> at 1640 and 1545 cm<sup>-1</sup> due to the formation of pyridinium. While OH-bound pyridine (weakly Brønsted acid sites) was observed at 1595, 1575, 1490 and 1445 cm<sup>-1</sup> due to the ν<sub>8a</sub>, ν<sub>8b</sub>, ν<sub>19a</sub> and ν<sub>19b</sub> vibrations. The acid concentration was determined after evacuation at 150 °C with the integrated molar extinction coefficients as reported by Emeis ε<sub>1455</sub> = 2.22; ε<sub>1545</sub> = 1.67 [26].

Temperature programmed desorption of ammonia (NH<sub>3</sub>-TPD) was performed on a Micromeritics AutoChem II supplied with a thermal conductivity detector (TCD) calibrated for NH<sub>3</sub>. In a typical experiment, 100 mg of catalyst was dried in a He flow for 1 h at 600 °C (ramp 10 °C/min). Subsequently, the temperature was decreased to 100 °C, after which NH<sub>3</sub> (10 vol% in He) was adsorbed pulsewise until oversaturation occurred. Physisorbed NH<sub>3</sub> was removed by flowing He for 2 h at 100 °C. Subsequently, NH<sub>3</sub> desorption was measured until 550 °C (ramp 10 °C/min).

### 3.3.1. Catalytic Testing

Propene oxidation was performed in a quartz fixed bed reactor (i.d. 4 mm) loaded with 150 mg of the catalyst (sieve fraction of 90–212 μm) and diluted with 300 mg SiC (sieve fraction 212–425 μm). Prior to catalysis the catalysts were reduced at 250 °C under 10% H<sub>2</sub> in He for 1 h. The reaction was carried out at 200 °C with a typical gas feed of 25 mL/min in total, with a volumetric concentration of 10% of H<sub>2</sub>, 10% O<sub>2</sub> and 10% C<sub>3</sub>H<sub>6</sub> in He as balance at a flow of 10,000 mL/g<sub>cat</sub>/h. Reaction products were quantified with a standard gas mixture with known concentrations using an online Interscience Compact GC 4.0 (analysis time 8 min) equipped with a Porabond Q column and a Molsieve 5A column in two separate channels, both with a thermal conductivity detector. The materials that did not contain gold did not show any activity at the studied conditions.

The conversion of propylene at reaction time *i* was calculated from the sum of moles of carbon in the effluent gas, denoted C<sub>oxygenates</sub> in all oxidized products (propylene oxide, propanal, acetone, acrolein, acetaldehyde and CO<sub>2</sub>/CO), with *n* as the number of moles of carbon and *χ* as conversion in % as:

$$\chi_{C_3H_6}(\%) = \frac{\sum nC_{oxygenates_i}}{nC_{feed_0}} \cdot 100\%$$

The selectivities in % towards the produced propylene oxide and other oxygenates at reaction time *i* were calculated as:

$$S_{PO}(\%) = \frac{nC_{PO_i}}{\sum nC_{oxygenates_i}} \cdot 100\%$$

$$S_{Product}(\%) = \frac{nC_{Product_i}}{\sum nC_{oxygenates_i}} \cdot 100\%$$

The conversion of hydrogen in % was calculated from the moles of H<sub>2</sub> in the effluent gas divided by the moles of H<sub>2</sub> in the feed as:

$$\chi_{H_2}(\%) = \frac{nH_{2_i}}{nH_{2_0}} \cdot 100\%$$

### 3.3.2. Stacked Bed Experiments

Stacked bed experiments were performed in a lab scale quartz fixed bed reactor (i.d. 4 mm) loaded with 75 mg of the Au/TS-1 catalyst (sieve fraction of 90–212 μm) that was diluted with 300 mg SiC (sieve fraction 212–425 μm) placed on top of a layer of 150 mg

of the support materials (sieve fraction 90–212  $\mu\text{m}$ ). Prior to the test the materials were reduced at 250 °C under 10%  $\text{H}_2$  in He for 1 h. The reaction was carried out at 200 °C with a typical gas feed of 25 mL/min in total, with a volumetric concentration of 10% of  $\text{H}_2$ , 10%  $\text{O}_2$  and 10%  $\text{C}_3\text{H}_6$  in He as balance at a flow of 10,000 mL/g<sub>support</sub>/h. Reaction products were quantified with a standard gas mixture with known concentrations using an online Interscience Compact GC 4.0 (analysis time 8 min) equipped with a Porabond Q column and a Molsieve 5A column in two separate channels, both with a thermal conductivity detector.

### 3.3.3. Turnover Frequency Determination

The turnover frequency is defined as the moles of propene that are converted per mole surface Au atoms per second [54].

$$\text{TOF (s}^{-1}\text{)} = \frac{r_{\text{C}_3\text{H}_6}}{n_{\text{Au}}}$$

The number of surface Au atoms is based on TEM and ICP analysis.

$$n_{\text{Au}} (\text{Au}_{\text{surface atoms}} \cdot \text{g}_{\text{cat}}^{-1}) = \frac{m_{\text{cat}} \cdot \text{Au-loading} \cdot D}{\text{MW}_{\text{Au}}}$$

The volume–area mean diameter (dVA) of the gold nanoparticles is based on counting typically 100–200 individual particles in TEM images.

$$dVA (A) = \frac{\sum n_i \cdot d_i^3}{\sum n_i \cdot d_i^2}$$

The dispersion D is determined as fraction of Au atoms at the surface of hemispherical nanoparticles.  $V_{\text{Au}}$  is the volume of a Au atom in the bulk (16.94  $\text{\AA}^3$ ) and  $A_{\text{Au}}$  is the area of a Au surface atom (8.75  $\text{\AA}^2$ )

$$D = \frac{6 \cdot \left( \frac{V_{\text{Au}}}{A_{\text{Au}}} \right)}{dVA}$$

## 4. Conclusions

To conclude, this study for the first time gives an overview of the role of metal oxide supports in the Au catalyzed propene epoxidation reaction in the presence of  $\text{H}_2$ . A first prerequisite is the formation of peroxides, which is much more pronounced on several of the investigated catalysts than on the established ones. However, a next requirement is the cooperativity between the gold nanoparticles and the metal oxide support to allow epoxidation of propene. The investigated metal oxide supported gold catalysts show moderate to high propene oxidation activity, but their selectivity towards PO is low. We observed that supports catalyze subsequent reactions of PO. In particular, metal oxides with a strong acidic character catalyze the isomerization of PO to propanal and acetone, while readily reducible supports show combustion of PO. A requirement for the metal oxide supports to achieve high epoxide selectivity is hence the presence of inert surface sites, a low specific surface area and/or low density of surface -OH groups. Interestingly,  $\text{Ti}^{4+}$ -based supports react with PO, but their use is necessary to achieve high epoxidation activity, selectivity and stability. With this research we show the impact of the support on the selectivity of the final catalysts and provide practical guidelines for the preparation of active and selective PO producing catalysts.

**Supplementary Materials:** The following supporting information can be downloaded at: <https://www.mdpi.com/article/10.3390/catal12030327/s1>. Figure S1. Additional High Angle Annular Dark Field Scanning Transmission Electron Microscopy images of the indicated metal oxide supported gold catalysts; Figure S2. Diffuse Reflectance UV-Vis absorbance spectra of the supported Au catalysts; Figure S3. Point-of-zero-charge determinations of the supported Au catalysts using a 0.1 M KCl solution. Dashed lines were drawn to guide the eye; Figure S4.  $\text{N}_2$  physisorption isotherms of the

indicated metal oxide supports. The darker colored symbols represents the adsorption isotherm and faded symbols represent desorption isotherm. The TS-1U represents the TS-1 sample before a thermal decomposition step at 500 °C; Figure S5. Conversion during propene (a) and hydrogen (b) oxidation over supported gold catalysts. Conditions: 150 mg of catalyst, 10,000 mL/gcat/h flow of 10% of each C<sub>3</sub>H<sub>6</sub>, O<sub>2</sub> and H<sub>2</sub> in He at 200–225 °C. 25 mg of Au/CeO<sub>2</sub> was used; Figure S6. Au/TiO<sub>2</sub> catalyst in propene epoxidation propene conversion at 100 °C (a) and thermogravimetric analysis of the Au/TiO<sub>2</sub> before catalysis (b) and after the catalytic test (c); Figure S7. Representative Transmission Electron Microscopy micrographs of Au/TiO<sub>2</sub> before (a) and after catalytic propene epoxidation (b). The scalebar indicates 20 nm; Table S1. Oxidation of propene at 200 °C in the presence of the supported gold catalysts.

**Author Contributions:** E.J.J.d.B.: catalyst synthesis, characterization, catalytic testing, writing and editing. B.J.F.: catalyst synthesis, catalyst testing. M.T.: electron microscopy characterization. B.D.: supervision, reviewing. P.E.d.J.: supervision, writing, reviewing and editing. All authors have read and agreed to the published version of the manuscript.

**Funding:** This research received no external funding.

**Data Availability Statement:** All data are shown in this manuscript or the supplementary materials.

**Acknowledgments:** Utrecht University is acknowledged for funding this project. Dennie Wezendonk is acknowledged for the TGA. The authors thank Claudia Keijzer for acquiring the SEM images and Luc Smulders for the NH<sub>3</sub>-TPD experiments. The MCC physisorption team is acknowledged for the N<sub>2</sub> physisorption.

**Conflicts of Interest:** The authors declare no conflict of interest.

## References

1. Trent, D.L. Propylene Oxide. In *Kirk-Othmer Encyclopedia of Chemical Technology*; Wiley: New York, NY, USA, 2001; ISBN 9780471238966.
2. Nijhuis, T.A.; Makkee, M.; Moulijn, J.A.; Weckhuysen, B.M. The production of propene oxide: Catalytic processes and recent developments. *Ind. Eng. Chem. Res.* **2006**, *45*, 3447–3459. [[CrossRef](#)]
3. Hayashi, T.; Tanaka, K.; Haruta, M. Selective Vapor-Phase Epoxidation of Propylene over Au/TiO<sub>2</sub> Catalysts in the Presence of Oxygen and Hydrogen. *J. Catal.* **1998**, *178*, 566–575. [[CrossRef](#)]
4. Chen, J.; Halin, S.J.A.; Schouten, J.C.; Nijhuis, T.A. Kinetic study of propylene epoxidation with H<sub>2</sub> and O<sub>2</sub> over Au/Ti-SiO<sub>2</sub> in the explosive regime. *Faraday Discuss.* **2011**, *152*, 321–336. [[CrossRef](#)] [[PubMed](#)]
5. Joshi, A.M.; Delgass, W.N.; Thomson, K.T. Partial oxidation of propylene to propylene oxide over a neutral gold trimer in the gas phase: A density functional theory study. *J. Phys. Chem. B* **2006**, *110*, 2572–2581. [[CrossRef](#)] [[PubMed](#)]
6. Uphade, B.S.; Akita, T.; Nakamura, T.; Haruta, M. Vapor-phase epoxidation of propene using H<sub>2</sub> and O<sub>2</sub> over Au/Ti-MCM-48. *J. Catal.* **2002**, *209*, 331–340. [[CrossRef](#)]
7. Chowdhury, B.; Bravo-Suárez, J.J.; Mimura, N.; Jiqing, L.; Bando, K.K.; Tsubota, S.; Haruta, M. In situ UV-vis and EPR study on the formation of hydroperoxide species during direct gas phase propylene epoxidation over Au/Ti-SiO<sub>2</sub> catalyst. *J. Phys. Chem. B* **2006**, *110*, 22995–22999. [[CrossRef](#)] [[PubMed](#)]
8. Nijhuis, T.A.; Visser, T.; Weckhuysen, B.M. Mechanistic Study into the Direct Epoxidation of Propene over Gold/Titania Catalysts. *J. Phys. Chem. B* **2005**, *109*, 19309–19319. [[CrossRef](#)]
9. Sinha, A.K.; Seelan, S.; Tsubota, S.; Haruta, M. Catalysis by Gold Nanoparticles: Epoxidation of Propene. *Top. Catal.* **2004**, *29*, 95–102. [[CrossRef](#)]
10. Lee, W.S.; Cem Akatay, M.; Stach, E.A.; Ribeiro, F.H.; Nicholas Delgass, W. Reproducible preparation of Au/TS-1 with high reaction rate for gas phase epoxidation of propylene. *J. Catal.* **2012**, *287*, 178–189. [[CrossRef](#)]
11. Gaudet, J.; Bando, K.K.; Song, Z.; Fujitani, T.; Zhang, W.; Su, D.S.; Oyama, S.T. Effect of gold oxidation state on the epoxidation and hydrogenation of propylene on Au/TS-1. *J. Catal.* **2011**, *280*, 40–49. [[CrossRef](#)]
12. Kropp, T.; Mavrikakis, M. Brønsted–Evans–Polanyi relation for CO oxidation on metal oxides following the Mars–van Krevelen mechanism. *J. Catal.* **2019**, *377*, 577–581. [[CrossRef](#)]
13. Doornkamp, C.; Ponec, V. The universal character of the Mars and Van Krevelen mechanism. *J. Mol. Catal. A Chem.* **2000**, *162*, 19–32. [[CrossRef](#)]
14. Gaálová, J.; Topka, P. Gold and ceria as catalysts for voc abatement: A review. *Catalysts* **2021**, *11*, 789. [[CrossRef](#)]
15. Delannoy, L.; Fajerweg, K.; Lakshmanan, P.; Potvin, C.; Méthivier, C.; Louis, C. Supported gold catalysts for the decomposition of VOC: Total oxidation of propene in low concentration as model reaction. *Appl. Catal. B Environ.* **2010**, *94*, 117–124. [[CrossRef](#)]
16. Chen, S.; Luo, L.; Jiang, Z.; Huang, W. Size-dependent reaction pathways of low-temperature CO oxidation on Au/CeO<sub>2</sub> catalysts. *ACS Catal.* **2015**, *5*, 1653–1662. [[CrossRef](#)]

17. Helali, Z.; Jedidi, A.; Syzgantseva, O.A.; Calatayud, M.; Minot, C. Scaling reducibility of metal oxides. *Theor. Chem. Acc.* **2017**, *136*, 1–16. [[CrossRef](#)]
18. Pinto, F.M.; Suzuki, V.Y.; Silva, R.C.; La Porta, F.A. Oxygen Defects and Surface Chemistry of Reducible Oxides. *Front. Mater.* **2019**, *6*, 260. [[CrossRef](#)]
19. Hernández-Ramírez, E.; Wang, J.A.; Chen, L.F.; Valenzuela, M.A.; Dalai, A.K. Partial oxidation of methanol catalyzed with Au/TiO<sub>2</sub>, Au/ZrO<sub>2</sub> and Au/ZrO<sub>2</sub>-TiO<sub>2</sub> catalysts. *Appl. Surf. Sci.* **2017**, *399*, 77–85. [[CrossRef](#)]
20. Aguado, J.; Escola, J.M.; Castro, M.C.; Paredes, B. Metathesis of 1-hexene over rhenium oxide supported on ordered mesoporous aluminas: Comparison with Re<sub>2</sub>O<sub>7</sub>/γ-Al<sub>2</sub>O<sub>3</sub>. *Appl. Catal. A Gen.* **2005**, *284*, 47–57. [[CrossRef](#)]
21. Osman, A.I.; Abu-Dahrieh, J.K.; Rooney, D.W.; Halawy, S.A.; Mohamed, M.A.; Abdelkader, A. Effect of precursor on the performance of alumina for the dehydration of methanol to dimethyl ether. *Appl. Catal. B Environ.* **2012**, *127*, 307–315. [[CrossRef](#)]
22. Ma, X.; Gong, J.; Wang, S.; Gao, N.; Wang, D.; Yang, X.; He, F. Reactivity and surface properties of silica supported molybdenum oxide catalysts for the transesterification of dimethyl oxalate with phenol. *Catal. Commun.* **2004**, *5*, 101–106. [[CrossRef](#)]
23. Nakajima, K.; Baba, Y.; Noma, R.; Kitano, M.; Kondo, J.N.; Hayashi, S.; Hara, M. Nb<sub>2</sub>O<sub>5</sub>·nH<sub>2</sub>O as a heterogeneous catalyst with water-tolerant lewis acid sites. *J. Am. Chem. Soc.* **2011**, *133*, 4224–4227. [[CrossRef](#)] [[PubMed](#)]
24. Dos Santos, C.G.; Marquez, D.T.; Crites, C.O.L.; Netto-Ferreira, J.C.; Scaiano, J.C. Plasmon heating mediated Friedel-Crafts alkylation of anisole using supported AuNP@Nb<sub>2</sub>O<sub>5</sub> catalysts. *Tetrahedron Lett.* **2017**, *58*, 427–431. [[CrossRef](#)]
25. Tao, Y.; De Luca, O.; Singh, B.; Kamphuis, A.J.; Chen, J.; Rudolf, P.; Pescarmona, P.P. WO<sub>3</sub>-SiO<sub>2</sub> nanomaterials synthesized using a novel template-free method in supercritical CO<sub>2</sub> as heterogeneous catalysts for epoxidation with H<sub>2</sub>O<sub>2</sub>. *Mater. Today Chem.* **2020**, *18*, 100373. [[CrossRef](#)]
26. Emeis, C.A. Determination of integrated molar extinction coefficients for infrared absorption bands of pyridine adsorbed on solid acid catalysts. *J. Catal.* **1993**, *141*, 347–354. [[CrossRef](#)]
27. Zalac, S.; Kallay, N. Application of mass titration to the point of zero charge determination. *J. Colloid Interface Sci.* **1992**, *149*, 233–240. [[CrossRef](#)]
28. Bravo-Suárez, J.J.; Bando, K.K.; Lu, J.; Haruta, M.; Fujitani, T.; Oyama, S.T. Transient technique for identification of true reaction intermediates: Hydroperoxide species in propylene epoxidation on gold/titanosilicate catalysts by X-ray absorption fine structure spectroscopy. *J. Phys. Chem. C* **2008**, *112*, 1115–1123. [[CrossRef](#)]
29. Xiong, G.; Cao, Y.; Guo, Z.; Jia, Q.; Tian, F.; Liu, L. The roles of different titanium species in TS-1 zeolite in propylene epoxidation studied by in situ UV Raman spectroscopy. *Phys. Chem. Chem. Phys.* **2016**, *18*, 190–196. [[CrossRef](#)]
30. Spanó, E.; Tabacchi, G.; Gamba, A.; Fois, E. On the role of Ti(IV) as a lewis acid in the chemistry of titanium zeolites: Formation, structure, reactivity, and aging of ti-peroxo oxidizing intermediates. A first principles study. *J. Phys. Chem. B* **2006**, *110*, 21651–21661. [[CrossRef](#)]
31. Sheldon, R.A.; Wallau, M.; Arends, I.W.C.E.; Schuchardt, U. Heterogeneous Catalysts for Liquid-Phase Oxidations: Philosophers' Stones or Trojan Horses? *Acc. Chem. Res.* **1998**, *31*, 485–493. [[CrossRef](#)]
32. Ghosh, S.; Acharyya, S.S.; Tiwari, R.; Sarkar, B.; Singha, R.K.; Pendem, C.; Sasaki, T.; Bal, R. Selective oxidation of propylene to propylene oxide over silver-supported tungsten oxide nanostructure with molecular oxygen. *ACS Catal.* **2014**, *4*, 2169–2174. [[CrossRef](#)]
33. Choudhary, V.R.; Patil, N.S.; Bhargava, S.K. Epoxidation of styrene by anhydrous H<sub>2</sub>O<sub>2</sub> over TS-1 and γ-Al<sub>2</sub>O<sub>3</sub> catalysts: Effect of reaction water, poisoning of acid sites and presence of base in the reaction mixture. *Catal. Lett.* **2003**, *89*, 55–62. [[CrossRef](#)]
34. Solsona, B.E.; Edwards, J.K.; Landon, P.; Carley, A.F.; Herzing, A.; Kiely, C.J.; Hutchings, G.J. Direct synthesis of hydrogen peroxide from H<sub>2</sub> and O<sub>2</sub> using Al<sub>2</sub>O<sub>3</sub> supported Au-Pd catalysts. *Chem. Mater.* **2006**, *18*, 2689–2695. [[CrossRef](#)]
35. Jildeh, Z.B.; Oberländer, J.; Kirchner, P.; Wagner, P.H.; Schöning, M.J. Thermocatalytic behavior of manganese (IV) oxide as nanoporous material on the dissociation of a gas mixture containing hydrogen peroxide. *Nanomaterials* **2018**, *8*, 262. [[CrossRef](#)] [[PubMed](#)]
36. Sheldon, R.A. Synthetic and mechanistic aspects of metal-catalysed epoxidations with hydroperoxides. *J. Mol. Catal.* **1980**, *7*, 107–126. [[CrossRef](#)]
37. Nijhuis, T.A.; Huizinga, B.J.; Makkee, M.; Moulijn, J.A. Direct Epoxidation of Propene Using Gold Dispersed on TS-1 and Other Titanium-Containing Supports. *Ind. Eng. Chem. Res.* **1999**, *38*, 884–891. [[CrossRef](#)]
38. van den Reijen, J.E.; Kanungo, S.; Welling, T.A.J.; Versluijs-Helder, M.; Nijhuis, T.A.; de Jong, K.P.; de Jongh, P.E. Preparation and particle size effects of Ag/α-Al<sub>2</sub>O<sub>3</sub> catalysts for ethylene epoxidation. *J. Catal.* **2017**, *356*, 65–74. [[CrossRef](#)]
39. Mao, C.-F.; Albert Vannice, M. High surface area α-aluminas III. Oxidation of ethylene, ethylene oxide, and acetaldehyde over silver dispersed on high surface area α-alumina. *Appl. Catal. A Gen.* **1995**, *122*, 61–76. [[CrossRef](#)]
40. Lu, J.; Bravo-Suárez, J.J.; Haruta, M.; Oyama, S.T. Direct propylene epoxidation over modified Ag/CaCO<sub>3</sub> catalysts. *Appl. Catal. A Gen.* **2006**, *302*, 283–295. [[CrossRef](#)]
41. Zemichael, F.W.; Palermo, A.; Tikhov, M.S.; Lambert, R.M. Propene epoxidation over K-promoted Ag/CaCO<sub>3</sub> catalysts: The effect of metal particle size. *Catal. Lett.* **2002**, *80*, 93–98. [[CrossRef](#)]
42. Teržan, J.; Djinović, P.; Zavašnik, J.; Arčon, I.; Žerjav, G.; Spreitzer, M.; Pintar, A. Alkali and earth alkali modified CuOx/SiO<sub>2</sub> catalysts for propylene partial oxidation: What determines the selectivity? *Appl. Catal. B Environ.* **2018**, *237*, 214–227. [[CrossRef](#)]
43. He, J.; Zhai, Q.; Zhang, Q.; Deng, W.; Wang, Y. Active site and reaction mechanism for the epoxidation of propylene by oxygen over CuOx/SiO<sub>2</sub> catalysts with and without Cs + modification. *J. Catal.* **2013**, *299*, 53–66. [[CrossRef](#)]

44. Diekmann, M.; Koch, G.; König, M.; Ressler, T. Correlation between Copper Oxide Particle Size and Selectivity towards Propylene Oxide in Selective Oxidation of Propene. *ChemCatChem* **2018**, *10*, 5459–5467. [[CrossRef](#)]
45. Mul, G.; Zwijnenburg, A.; van der Linden, B.; Makkee, M.; Moulijn, J.A. Stability and Selectivity of Au/TiO<sub>2</sub> and Au/TiO<sub>2</sub>/SiO<sub>2</sub> Catalysts in Propene Epoxidation: An in Situ FT-IR Study. *J. Catal.* **2001**, *201*, 128–137. [[CrossRef](#)]
46. Ruiz, A.; van der Linden, B.; Makkee, M.; Mul, G. Acrylate and propoxy-groups: Contributors to deactivation of Au/TiO<sub>2</sub> in the epoxidation of propene. *J. Catal.* **2009**, *266*, 286–290. [[CrossRef](#)]
47. Sinha, A.K.; Seelan, S.; Akita, T.; Tsubota, S.; Haruta, M. Vapor phase propylene epoxidation over Au/Ti-MCM-41 catalysts prepared by different Ti incorporation modes. *Appl. Catal. A Gen.* **2003**, *240*, 243–252. [[CrossRef](#)]
48. Stangland, E.E.; Taylor, B.; Andres, R.P.; Delgass, W.N. Direct Vapor Phase Propylene Epoxidation over Deposition-Precipitation Gold-Titania Catalysts in the Presence of H<sub>2</sub>/O<sub>2</sub>: Effects of Support, Neutralizing Agent, and Pretreatment. *J. Phys. Chem. B* **2005**, *109*, 2321–2330. [[CrossRef](#)]
49. Harris, J.W.; Arvay, J.; Mitchell, G.; Delgass, W.N.; Ribeiro, F.H. Propylene oxide inhibits propylene epoxidation over Au/TS-1. *J. Catal.* **2018**, *365*, 105–114. [[CrossRef](#)]
50. de Boed, E.J.J.; de Rijk, J.W.; de Jongh, P.E.; Donoeva, B. Steering the Selectivity in Gold–Titanium-Catalyzed Propene Oxidation by Controlling the Surface Acidity. *J. Phys. Chem. C* **2021**, *125*, 16557–16568. [[CrossRef](#)]
51. Zanella, R.; Delannoy, L.; Louis, C. Mechanism of deposition of gold precursors onto TiO<sub>2</sub> during the preparation by cation adsorption and deposition-precipitation with NaOH and urea. *Appl. Catal. A Gen.* **2005**, *291*, 62–72. [[CrossRef](#)]
52. Zhu, H.; Liang, C.; Yan, W.; Overbury, S.H.; Dai, S. Preparation of highly active silica-supported Au catalysts for Co oxidation by a solution-based technique. *J. Phys. Chem. B* **2006**, *110*, 10842–10848. [[CrossRef](#)] [[PubMed](#)]
53. Yin, H.; Ma, Z.; Overbury, S.H.; Dai, S. Promotion of Au(en)<sub>2</sub>Cl<sub>3</sub>-Derived Au/Fumed SiO<sub>2</sub> by Treatment with KMnO<sub>4</sub>. *Society* **2008**, *2*, 8349–8358. [[CrossRef](#)]
54. Feng, X.; Duan, X.; Qian, G.; Zhou, X.; Chen, D.; Yuan, W. Insights into size-dependent activity and active sites of Au nanoparticles supported on TS-1 for propene epoxidation with H<sub>2</sub> and O<sub>2</sub>. *J. Catal.* **2014**, *317*, 99–104. [[CrossRef](#)]
55. Stangland, E.E.; Stavens, K.B.; Andres, R.P.; Delgass, W.N. Characterization of gold-titania catalysts via oxidation of propylene to propylene oxide. *J. Catal.* **2000**, *191*, 332–347. [[CrossRef](#)]
56. Kanungo, S.; Perez Ferrandez, D.M.; Neira D'Angelo, F.; Schouten, J.C.; Nijhuis, T.A. Kinetic study of propene oxide and water formation in hydro-epoxidation of propene on Au/Ti-SiO<sub>2</sub> catalyst. *J. Catal.* **2016**, *338*, 284–294. [[CrossRef](#)]
57. Barton, D.G.; Podkolzin, S.G. Kinetic study of a direct water synthesis over silica-supported gold nanoparticles. *J. Phys. Chem. B* **2005**, *109*, 2262–2274. [[CrossRef](#)]
58. Nijhuis, T.A.; Sacaliuc, E.; Beale, A.M.; van der Eerden, A.M.J.; Schouten, J.C.; Weckhuysen, B.M. Spectroscopic evidence for the adsorption of propene on gold nanoparticles during the hydro-epoxidation of propene. *J. Catal.* **2008**, *258*, 256–264. [[CrossRef](#)]
59. Aneggi, E.; Boaro, M.; De Leitenburg, C.; Dolcetti, G.; Trovarelli, A. Insights into the redox properties of ceria-based oxides and their implications in catalysis. *J. Alloys Compd.* **2006**, *408–412*, 1096–1102. [[CrossRef](#)]
60. Haruta, M.; Uphade, B.S.; Tsubota, S.; Miyamoto, A. Selective oxidation of propylene over gold deposited on titanium-based oxides. *Res. Chem. Intermed.* **1998**, *24*, 329–336. [[CrossRef](#)]
61. Huang, J.; Takei, T.; Ohashi, H.; Haruta, M. Propene epoxidation with oxygen over gold clusters: Role of basic salts and hydroxides of alkalis. *Appl. Catal. A Gen.* **2012**, *435–436*, 115–122. [[CrossRef](#)]
62. Cant, N.W.; Hall, W.K. Catalytic oxidation. IV. Ethylene and propylene oxidation over gold. *J. Phys. Chem.* **1971**, *75*, 2914–2921. [[CrossRef](#)]
63. Blues, E.T.; Bryce-Smith, D.; Lawston, I.W.; Wall, G.D. Gold(I) ketenide. *J. Chem. Soc. Chem. Commun.* **1974**, *13*, 513–514. [[CrossRef](#)]
64. McEwan, L.; Julius, M.; Roberts, S.; Fletcher, J.C.Q. A review of the use of gold catalysts in selective hydrogenation reactions. *Gold Bull.* **2010**, *43*, 298–306. [[CrossRef](#)]
65. Delannoy, L.; Chantry, R.L.; Casale, S.; Li, Z.Y.; Borensztein, Y.; Louis, C. HRTEM and STEM-HAADF characterisation of Au–TiO<sub>2</sub> and Au–Al<sub>2</sub>O<sub>3</sub> catalysts for a better understanding of the parameters influencing their properties in CO oxidation. *Phys. Chem. Chem. Phys.* **2013**, *15*, 3473. [[CrossRef](#)] [[PubMed](#)]
66. Suo, Z.; Jin, M.; Lu, J.; Wei, Z.; Li, C. Direct gas-phase epoxidation of propylene to propylene oxide using air as oxidant on supported gold catalyst. *J. Nat. Gas Chem.* **2008**, *17*, 184–190. [[CrossRef](#)]
67. Thornburg, N.E.; Thompson, A.B.; Notestein, J.M. Periodic Trends in Highly Dispersed Groups IV and V Supported Metal Oxide Catalysts for Alkene Epoxidation with H<sub>2</sub>O<sub>2</sub>. *ACS Catal.* **2015**, *5*, 5077–5088. [[CrossRef](#)]
68. Zaki, M.I.; Hussein, G.A.M.; Mansour, S.A.A.; El-Ammawy, H.A. Adsorption and surface reactions of pyridine on pure and doped ceria catalysts as studied by infrared spectroscopy. *J. Mol. Catal.* **1989**, *51*, 209–220. [[CrossRef](#)]
69. Longo, A.; de Boed, E.J.J.; Mammen, N.; van der Linden, M.; Honkala, K.; Häkkinen, H.; de Jongh, P.E.; Donoeva, B. Towards Atomically Precise Supported Catalysts from Monolayer-Protected Clusters: The Critical Role of the Support. *Chem. Eur. J.* **2020**, *26*, 7051–7058. [[CrossRef](#)]
70. Erdem, B.; Hunsicker, R.A.; Simmons, G.W.; David Sudol, E.; Dimonie, V.L.; El-Aasser, M.S. XPS and FTIR surface characterization of TiO<sub>2</sub> particles used in polymer encapsulation. *Langmuir* **2001**, *17*, 2664–2669. [[CrossRef](#)]
71. Zhuravlev, L.T. The surface chemistry of amorphous silica. Zhuravlev model. *Colloids Surf. A Physicochem. Eng. Asp.* **2000**, *173*, 1–38. [[CrossRef](#)]

72. Nguefack, M.; Popa, A.F.; Rossignol, S.; Kappenstein, C. Preparation of alumina through a sol-gel process. Synthesis, characterization, thermal evolution and model of intermediate boehmite. *Phys. Chem. Chem. Phys.* **2003**, *5*, 4279–4289. [[CrossRef](#)]
73. Hietala, J.; Root, A.; Knuutila, P. The surface acidity of pure and modified aluminas in Re/Al<sub>2</sub>O<sub>3</sub> metathesis catalysts as studied by 1H MAS NMR spectroscopy and its importance in the ethenolysis of 1,5-cyclooctadiene. *J. Catal.* **1994**, *150*, 46–55. [[CrossRef](#)]
74. McHale, J.M.; Auroux, A.; Perrotta, A.J.; Navrotsky, A. Surface energies and thermodynamic phase stability in nanocrystalline aluminas. *Science* **1997**, *277*, 788–789. [[CrossRef](#)]
75. Bigey, C.; Hilaire, L.; Maire, G. Catalysis on Pd/WO<sub>3</sub> and Pd/WO<sub>2</sub>: Effect of the modifications of the surface states due to redox treatments on the skeletal rearrangement of hydrocarbons. Part I. Physical and chemical characterizations of catalysts by BET, TPR, XRD, XAS, and XPS. *J. Catal.* **1999**, *184*, 406–420. [[CrossRef](#)]
76. Arends, I.W.C.E.; Sheldon, R.A. Activities and stabilities of heterogeneous catalysts in selective liquid phase oxidations: Recent developments. *Appl. Catal. A Gen.* **2001**, *212*, 175–187. [[CrossRef](#)]
77. Robinson, M.W.C.; Pillinger, K.S.; Graham, A.E. Highly efficient Meinwald rearrangement reactions of epoxides catalyzed by copper tetrafluoroborate. *Tetrahedron Lett.* **2006**, *47*, 5919–5921. [[CrossRef](#)]
78. Cumaratunge, L.; Delgass, W.N. Enhancement of Au capture efficiency and activity of Au/TS-1 catalysts for propylene epoxidation. *J. Catal.* **2005**, *232*, 38–42. [[CrossRef](#)]
79. Feng, X.; Yang, J.; Duan, X.; Cao, Y.; Chen, B.; Chen, W.; Lin, D.; Qian, G.; Chen, D.; Yang, C.; et al. Enhanced Catalytic Performance for Propene Epoxidation with H<sub>2</sub> and O<sub>2</sub> over Bimetallic Au–Ag/Uncalcined Titanium Silicate-1 Catalysts. *ACS Catal.* **2018**, *8*, 7799–7808. [[CrossRef](#)]
80. Cozzolino, M.; Di Serio, M.; Tesser, R.; Santacesaria, E. Grafting of titanium alkoxides on high-surface SiO<sub>2</sub> support: An advanced technique for the preparation of nanostructured TiO<sub>2</sub>/SiO<sub>2</sub> catalysts. *Appl. Catal. A Gen.* **2007**, *325*, 256–262. [[CrossRef](#)]
81. Chen, J.; Halin, S.J.A.; Pidko, E.A.; Verhoeven, M.W.G.M.T.; Ferrandez, D.M.P.; Hensen, E.J.M.; Schouten, J.C.; Nijhuis, T.A. Enhancement of Catalyst Performance in the Direct Propene Epoxidation: A Study into Gold-Titanium Synergy. *ChemCatChem* **2013**, *5*, 467–478. [[CrossRef](#)]
82. Lu, X.; Zhao, G.; Lu, Y. Propylene epoxidation with O<sub>2</sub> and H<sub>2</sub>: A high-performance Au/TS-1 catalyst prepared via a deposition-precipitation method using urea. *Catal. Sci. Technol.* **2013**, *3*, 2906–2909. [[CrossRef](#)]
83. Lee, W.S.; Cem Akatay, M.; Stach, E.A.; Ribeiro, F.H.; Nicholas Delgass, W. Gas-phase epoxidation of propylene in the presence of H<sub>2</sub> and O<sub>2</sub> over small gold ensembles in uncalcined TS-1. *J. Catal.* **2014**, *313*, 104–112. [[CrossRef](#)]
84. Chowdhury, B.; Bravo-Suárez, J.J.; Daté, M.; Tsubota, S.; Haruta, M. Trimethylamine as a gas-phase promoter: Highly efficient epoxidation of propylene over supported gold catalysts. *Angew. Chemie Int. Ed.* **2006**, *45*, 412–415. [[CrossRef](#)] [[PubMed](#)]
85. Liu, H.; Lu, G.; Hu, H. Synthesis, characterization and catalytic performance of titanium silicalite-1 prepared in the presence of nonionic surfactants. *Mater. Chem. Phys.* **2006**, *100*, 162–167. [[CrossRef](#)]
86. Maschmeyer, T.; Rey, F.; Sankar, G.; Thomas, J.M. Heterogeneous catalysts obtained by grafting metallocene complexes onto mesoporous silica. *Nature* **1995**, *378*, 159–162. [[CrossRef](#)]
87. Block, B.P.; Bailar, J.C. The Reaction of Gold(III) with Some Bidentate Coördinating Groups<sup>1</sup>. *J. Am. Chem. Soc.* **1951**, *73*, 4722–4725. [[CrossRef](#)]